Cell Reports

Article

Self-maintenance of zonal hepatocytes during adult homeostasis and their complex plasticity upon distinct liver injuries

Graphical abstract

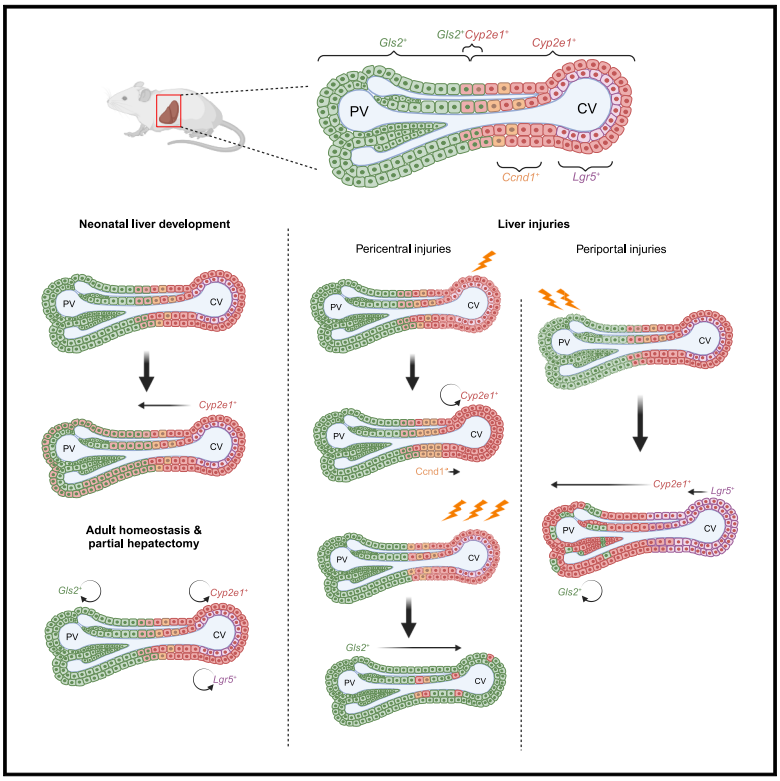

Highlights

- Pericentral *Lgr5*$^{-}$*Cyp2e1*$^{+}$ hepatocytes expand and fuel neonatal liver growth
- Distinct zonal hepatocyte subsets self-maintain during adult homeostasis
- Midlobular *Ccnd1*$^{+}$ hepatocytes are not necessary for adult liver regeneration
- While local repair is preferred, zonal hepatocytes harbor high plasticity upon liver injury

Authors

Chow Hiang Ang, Philip Arandjelovic, Jinming Cheng, ..., Yunshun Chen, David M. Virshup, Nai Yang Fu

Correspondence

fu@wehi.edu.au

In brief

Ang et al. develop multiple genetic lineage-tracing mouse models to systematically study liver regeneration. They demonstrate that pericentral *Cyp2e1*$^{+}$ hepatocytes fuel neonatal liver development. Distinct zonal hepatocytes self-maintain during adult homeostasis and partial hepatectomy. While local repair is preferred, zonal hepatocytes harbor high plasticity to replenish neighboring populations upon injuries.

Ang et al., 2025, Cell Reports *44*, 115093
January 28, 2025
https://doi.org/10.1016/j.celrep.2024.115093

CellPress

Cell Reports

CellPress
OPEN ACCESS

Article

Self-maintenance of zonal hepatocytes during adult homeostasis and their complex plasticity upon distinct liver injuries

Chow Hiang Ang,[1] Philip Arandjelovic,[2,3] Jinming Cheng,[2,3,4] Jicheng Yang,[1,2,3] Fusheng Guo,[1] Yuanquan Yu,[5] Sarmilla Nelameham,[1] Lachlan Whitehead,[3,6] Jiangtao Li,[5] David L. Silver,[7] Nick Barker,[8,9] Jane E. Visvader,[2,3] Pierce K.H. Chow,[10,12] Gordon K. Smyth,[4,11] Yunshun Chen,[2,3,4] David M. Virshup,[1] and Nai Yang Fu[1,2,3,9,13,*]

[1]Cancer and Stem Cell Biology Program, Duke-NUS Medical School, Singapore 169857, Singapore
[2]Cancer Biology and Stem Cells Division, The Walter and Eliza Hall Institute of Medical Research, Parkville, VIC 3052, Australia
[3]Department of Medical Biology, University of Melbourne, Parkville, VIC 3010, Australia
[4]Bioinformatics Division, The Walter and Eliza Hall Institute of Medical Research, Parkville, VIC 3052, Australia
[5]HPB Surgery, The Second Affiliated Hospital Zhejiang University School of Medicine, Hangzhou, China
[6]Advanced Technology and Biology Division, The Walter and Eliza Hall Institute of Medical Research, Parkville, VIC 3052, Australia
[7]Cardiovascular & Metabolic Disorders Program, Duke-NUS Medical School, Singapore 169857, Singapore
[8]Institute of Molecular and Cell Biology, Agency for Science, Technology, and Research (A*STAR), Singapore 138673, Singapore
[9]Department of Physiology, Yong Loo Lin School of Medicine, National University of Singapore, Singapore, Singapore
[10]Surgery Academic-Clinical Program, Duke-NUS Medical School, Singapore 169857, Singapore
[11]School of Mathematics and Statistics, University of Melbourne, Parkville, VIC 3010, Australia
[12]Department of Hepato-pancreato-biliary and Transplant Surgery, Division of Surgery and Surgical Oncology, Singapore General Hospital and National Cancer Centre Singapore, Singapore
[13]Lead contact
*Correspondence: fu@wehi.edu.au
https://doi.org/10.1016/j.celrep.2024.115093

SUMMARY

Hepatocytes are organized into distinct zonal subsets across the liver lobule, yet their contributions to liver homeostasis and regeneration remain controversial. Here, we developed multiple genetic lineage-tracing mouse models to systematically address this. We found that the liver lobule can be divided into two major zonal and molecular hepatocyte populations marked by *Cyp2e1* or *Gls2*. Pericentral *Cyp2e1*$^+$ and periportal *Gls2*$^+$ hepatocytes maintain their own lineage during adult homeostasis, while *Cyp2e1*$^+$ hepatocytes fuel neonatal liver growth. The *Gls2*$^+$ and *Cyp2e1*$^+$ populations can rapidly regenerate one another when one of the populations is severely damaged. Midlobular *Ccnd1*$^+$ hepatocytes are enriched in the *Cyp2e1*$^+$ zone in adult liver but have limited contributions to regeneration upon partial hepatectomy and severe pericentral injury. Remarkably, *Lgr5*$^+$ hepatocytes, a unique *Cyp2e1*$^+$ subset, contribute significantly to liver replenishment upon periportal injuries. Our findings unravel that zonal hepatocytes mainly self-maintain during homeostasis but exhibit complex plasticity in repair upon injury.

INTRODUCTION

Hepatocytes are the main cellular component of the liver, with an estimated lifespan of around 300 days in mice.[1,2] While they are largely quiescent during homeostasis, hepatocytes display an exceptional capability to rapidly restore liver mass upon injury. On the other hand, the neonatal liver grows at a tremendously rapid rate. Unlike other organs such as the small intestines or skin, where stem or progenitor cells are prominent, the existence of stem or progenitor cells in the liver has long been a topic of debate. There are two main epithelial cell lineages in the healthy adult liver, namely hepatocytes and cholangiocytes. In the long-standing streaming liver theory, the facultative stem cells that are believed to reside in the "canal of Hering" of the bile ducts in the portal area produce intermediate cells named "oval cells" that give rise to mature hepatocytes and contribute to liver maintenance as they stream from periportal to pericentral regions within the liver lobule.[3,4] However, recent evidence strongly suggests that the mass of the adult liver is primarily maintained by the self-renewal of pre-existing mature hepatocytes during normal homeostasis and in response to various liver injuries.[5,6] Meanwhile, cholangiocytes and/or oval cells likely give rise to hepatocytes under special circumstances, such as when hepatocyte proliferation is profoundly blocked,[7,8] hepatocytes are completely depleted,[9] or the liver is under severe long-term injury.[10]

The liver lobules are the functional units of the liver. Each liver lobule is hexagonal in shape and consists of a central vein surrounded by six portal triads that are constituted by the bile duct, portal vein, and hepatic artery. A "three-zone model," proposed a century ago, consists of the zone of permanent activity

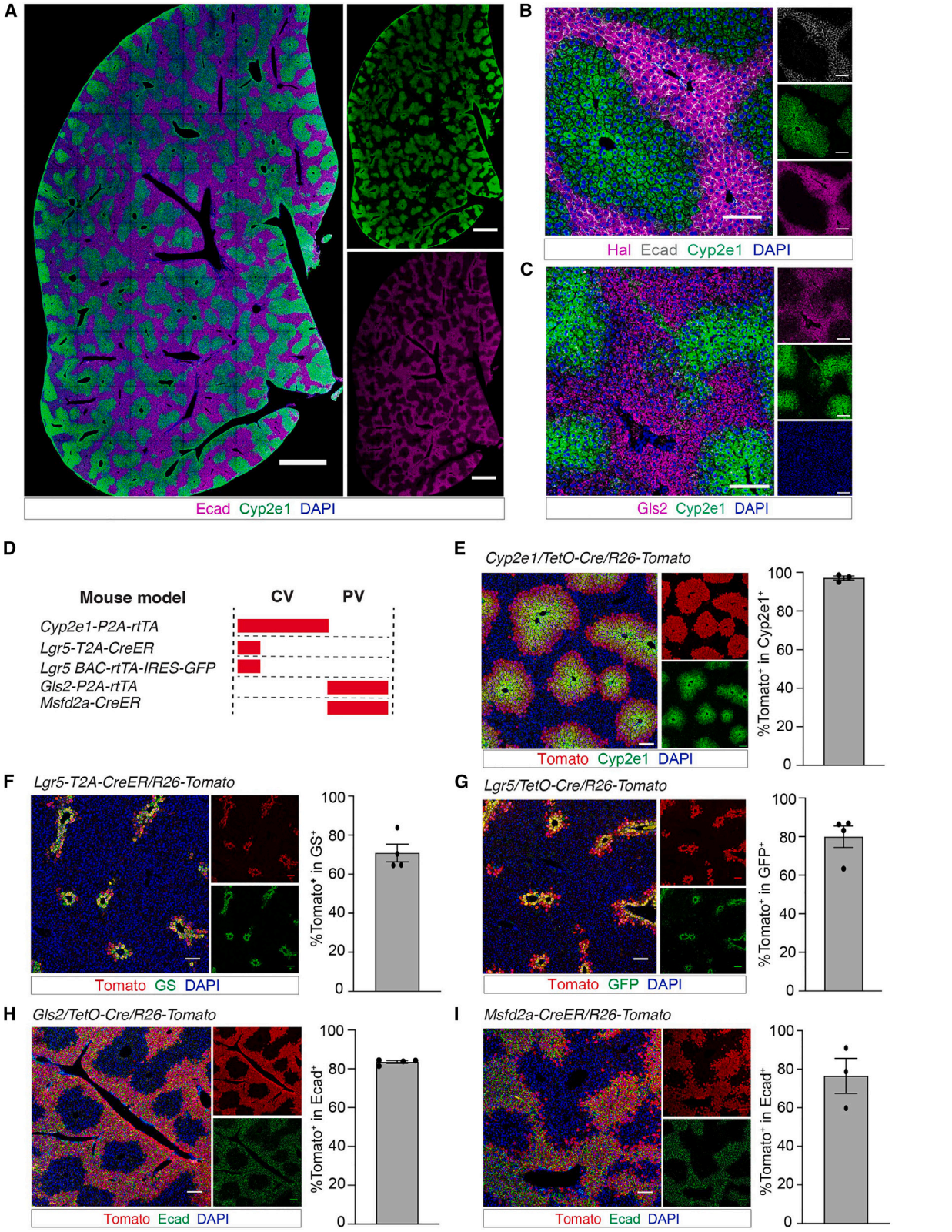

(legend on next page)

(periportal zone, or zone 1), the intermediary zone (zone 2), and the zone of permanent repose (pericentral zone, or zone 3).[11] Interestingly, the three-zone concept is still prevalent even though the original definition of the three regions is no longer accurate.[12] The term "zonation" now refers to the spatial location of hepatocytes with different metabolic functions along the lobular axis.[13] According to the typical three-zone model, zones 1 and 3 consist of 6–8 layers of periportal hepatocytes and several layers of pericentral hepatocytes, respectively.[14] However, the definition and function of zone 2 in the middle of the lobule are ambiguous.[14–16] In addition, recent single-cell RNA profiling studies have assigned hepatocytes across the liver lobule to nine molecular layers based on the expression of several landmark genes.[17,18]

Emerging evidence from lineage-tracing mouse models suggests that hepatocytes in different lobular zones may differ in their capacity to generate new hepatocytes during liver homeostasis and upon liver damage. For instance, *Axin2*$^+$ cells were observed in the pericentral zone in adult liver lobules[19,20] and contributed significantly to sustaining other hepatocytes during liver homeostasis.[21] However, more recent studies reported that *Axin2*$^+$ hepatocytes are insignificant in maintaining other hepatocytes in liver homeostasis and regeneration.[22,23] A small subset of hepatocytes adjacent to the portal veins labeled by *Sox9* gave rise to a significant proportion of new hepatocytes in response to different injuries.[24,25] The *Mfsd2a*$^+$ cells in the periportal zone were found to contribute significantly to the generation of new hepatocytes during injury-induced liver regeneration but slightly decreased during normal adult liver homeostasis.[26] The rare *Lgr5*$^+$ hepatocytes, closely adjacent to the central vein in normal liver, were found to be long lived and self-maintained during the postnatal lifespan.[27] More recently, midlobular hepatocytes in zone 2 are proposed to serve as a major cell reservoir during normal homeostasis and liver regeneration upon injury[28–30] as well as liver enlargement during pregnancy.[31] Genetic markers including *Hamp2*, *Igfbf2*, and *Ccnd1* were shown to label hepatocytes in zone 2 and were used to generate mouse models for lineage tracing. However, none of these markers truly defines a midlobular zone that is distinct from the two other zones. For instance, *Hamp2* is sparsely expressed across the liver lobule, with more *Hamp2*$^+$ cells in the middle area of the liver lobule.[29] Half of *Igfbf2*-labeled cells are found in the *Ecad*$^+$ periportal zone.[28] Furthermore, there is a possibility that other hepatocyte subpopulations, such as *Tert*^{high} cells, which are dispersed throughout the lobule,[32] also contribute significantly to homeostasis and regeneration. Due to this lack of clarity, a clear definition of distinct zonal hepatocytes, and the dynamics and role of zonal hepatocytes in liver homeostasis and regeneration require further investigation. Here, we developed and used multiple lineage-tracing mouse models to systematically address the cell fates and contribution of distinct zonal hepatocyte subsets during early neonatal liver development, normal adult homeostasis, and regeneration upon partial hepatectomy (PH) as well as different liver injuries.

RESULTS

The liver lobule can be separated into two major zones, marked by Cyp2e1 and Gls2

It has been proposed that the liver lobule consists of three main functional zones along a spatial axis from the portal to the central vein. As the midlobular zone 2 is less defined, we re-examined the three-zone concept closely by analyzing liver sections of adult wild-type mice via combined staining of various established zonal markers. Interestingly, we observed two main zones within the liver lobule with no gap between the areas, marked by the pericentral marker Cyp2e1 and periportal marker E-cadherin (Ecad) (Figure 1A). Co-staining of Cyp2e1 and two other periportal markers, Hal (Figure 1B) and Gls2 (Figure 1C), further indicates that the liver lobule is constituted by two distinct zones expressing Cyp2e1 and Ecad/Hal/Gls2, respectively. Hereafter, we refer to these two zones as the pericentral *Cyp2e1*$^+$ zone and the periportal *Gls2*$^+$ zone. It is important to note that a subset of hepatocytes within the *Cyp2e1*$^+$ zone, constituting 1–2 layers of cells most adjacent to the central vein, express a unique marker, GS, that distinguishes them from the rest of hepatocytes within the zone (Figure S1A). As previously reported,[27] this unique subset of hepatocytes is also specifically marked by the expression of *Lgr5*.

Generation of mouse models for conducting systematic lineage tracing of distinct zonal hepatocyte subsets

To characterize the molecular features and cell fates of hepatocytes in *Cyp2e1*$^+$ and *Gls2*$^+$ zones, we generated two new doxycycline (DOX)-inducible models, *Cyp2e1-P2A-rtTA* and *Gls2-P2A-rtTA*, by replacing the TGA stop codon of the endogenous *Cyp2e1* and *Gls2* genes with a P2A-rtTA cassette (Figure S1B). Western blot analysis showed that the expression of Cyp2e1 and Gls2 proteins remains intact and that P2A-mediated ribosome skipping is highly efficient in both lines (Figure S1D). We then crossed mice from these two lines to *TetO-Cre* and *Rosa26-Tomato* Cre reporter mice to generate *Cyp2e1/TetO-Cre/R26-Tomato* and *Gls2/TetO-Cre/R26-Tomato* models for cell labeling and lineage tracing (Figure S1B). To conduct systematic lineage tracing of distinct zonal hepatocyte subsets with defined spatial localization within the entire liver lobule, we included a DOX-inducible bacterial artificial chromosome (BAC) transgenic[27] and a tamoxifen (TAM)-inducible knockin Lgr5[33] model to label and trace *Lgr5*$^+$ hepatocytes within the *Cyp2e1*$^+$ zone. Additionally, we included a TAM-inducible model to trace periportal *Msfd2a*$^+$ hepatocytes[34] (Figure 1D).

Figure 1. Mouse models for labeling and lineage tracing of distinct zonal hepatocyte subsets

(A–C) Representative tile scan confocal image showing two main zones marked by the periportal and pericentral markers Ecad and Cyp2e1, respectively (A), and co-staining of Hal, Ecad, and Cyp2e1 (B) or Gls2 and Cyp2e1 (C) in the liver lobule of adult FVB mice.

(D) Representation of five different mouse models for labeling and tracing hepatocytes in three distinct zones of the liver lobule.

(E–I) Confocal images and quantification analysis showing the labeling efficiency in each lineage-tracing model as indicated. Error bars represent mean ± SEM. n = 3–4 mice. An average of 5,000 cells per site, 3–10 sites from the liver of each mouse were counted.

Scale bars: (A) 500 μm and (B, C, and E–I) 100 μm.

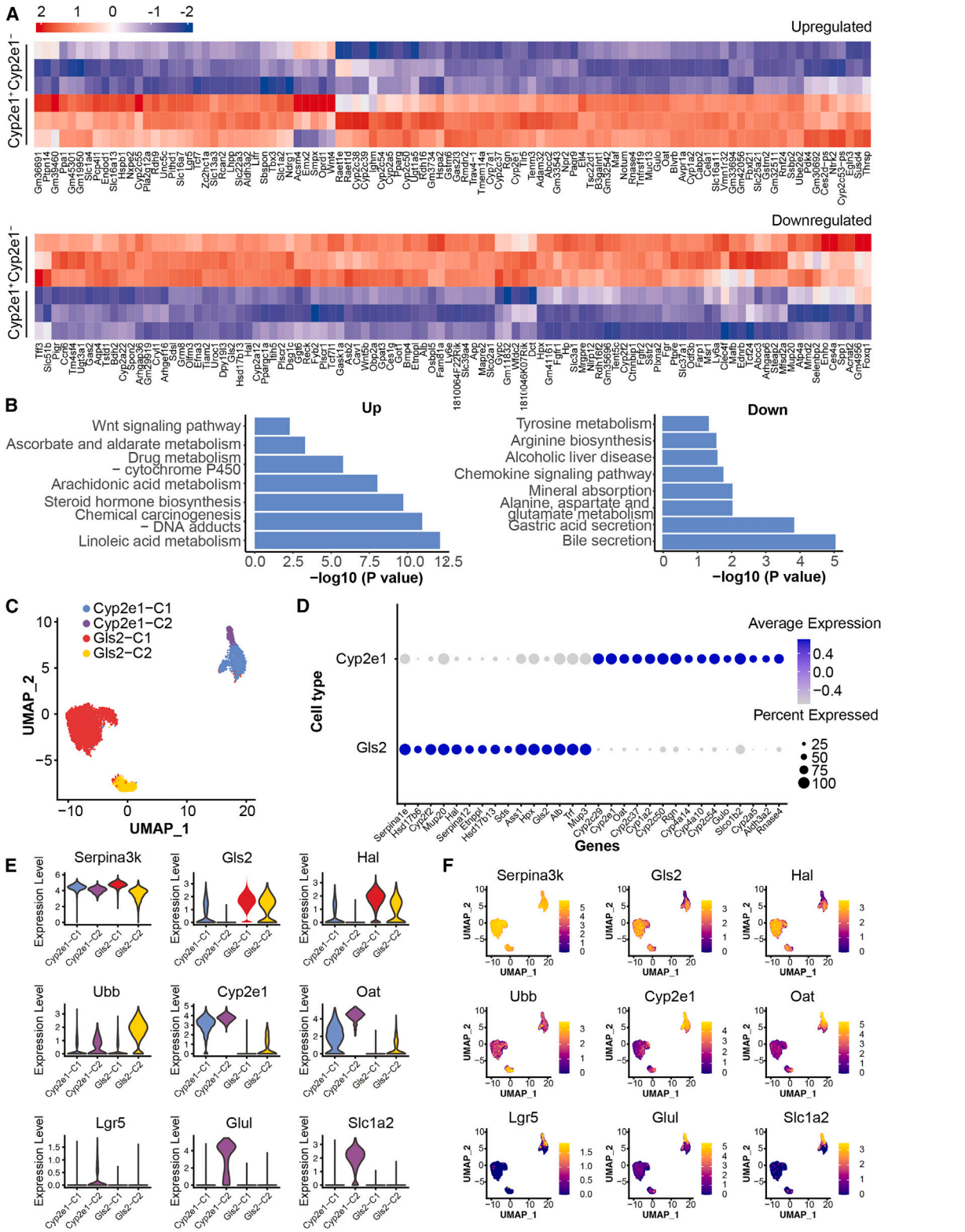

(legend on next page)

Next, we sought to determine the labeling efficiency and promoter fidelity in each mouse model. We first confirmed that Tomato is not expressed in any of these models if mice are not pulsed by DOX or TAM (Figures S1E–S1I). In contrast, all five models showed excellent labeling efficiencies and promoter fidelities when adult mice were induced with DOX or TAM and analyzed shortly after induction. Co-staining of Tomato and Cyp2e1 in liver sections of *Cyp2e1/TetO-Cre/R26-Tomato* mice showed that the Tomato$^+$ population highly overlapped with the Cyp2e1$^+$ population, in which almost all pericentral hepatocytes within the Cyp2e1$^+$ region express Tomato (Figure 1E). Notably, Tomato expression extended to 1–2 layers of hepatocytes at the boundary beyond the pericentral zone detected by the anti-Cyp2e1 antibody. This is likely because the expression of Cyp2e1 protein is beyond the detection limit of the anti-Cyp2e1 antibody in these hepatocytes, where it can still be marked by Tomato, which is controlled by the highly sensitive Cre reporter system.[35] Similarly, Tomato was found in approximately 70%–80% glutamine synthetase (GS)$^+$ hepatocytes and extended slightly beyond the GS$^+$ zone in the two Lgr5 lineage-tracing models (Figures 1F and 1G). In liver sections *of Gls2/TetO-Cre/R26-Tomato* and *Msfd2a-CreER/R26-Tomato* mice, Tomato expression was turned on in ~80% of the periportal Ecad$^+$ population and restricted to the population (Figures 1H and 1I).

Integration of gene expression signatures of zonal hepatocytes with single-cell RNA-seq data

To interrogate the molecular characteristics of the two major zones separated by the expression of *Cyp2e1*, we determined the gene expression profiles of Tomato$^+$ (*Cyp2e1*$^+$ zone) versus Tomato$^-$ (*Gls2*$^+$ zone) hepatocytes that were sorted by fluorescence-activated cell sorting (FACS) from adult *Cyp2e1/TetO-Cre/R26-Tomato* male mice treated with DOX for 1 week. 186 upregulated and 191 downregulated genes in Tomato$^+$ versus Tomato$^-$ hepatocytes were identified (Treat-false discovery rate (FDR) < 0.05; > 2-fold change). Typical pericentral genes, including *Cyp2e1*, *Oat*, and *Rnase4*, were highly upregulated in Tomato$^+$ cells. In contrast, periportal genes, such as *Gls2*, *Hal*, and *Cdh1*, were enriched in Tomato$^-$ cells (Figure 2A). KEGG analysis of differentially expressed genes (DEGs) revealed a significant enrichment of pathways associated with Wnt signaling, drug metabolism, steroid hormone biosynthesis, and chemical carcinogenesis in Tomato$^+$ hepatocytes. Conversely, Tomato$^-$ cells were enriched for genes involved in tyrosine, alanine, aspartate, and glutamate metabolism, chemokine signaling pathway, and gastric acid and bile secretion (Figure 2B). We then integrated the gene expression signatures of Tomato$^+$ and Tomato$^-$ cells with the single-cell RNA sequencing (RNA-seq) dataset that has been reported previously[36] and found that hepatocytes could be classified into two major distinct populations (Figure 2C). Most cells in the *Cyp2e1*$^+$ population highly expressed cytochrome P450 genes and many other pericentral markers (Figure 2D). In contrast, periportal genes were highly enriched in the Gls2 population. Interestingly, both *Cyp2e1* and *Gls2* populations could be further divided into two sub-clusters in this dataset (Figure 2C). *Lgr5*, *Glul*, and *Slc1a2*, which are well-characterized genetic markers for a rare subset adjacent to pericentral veins, were found to be exclusively expressed in Cyp2e1-C2 (Figures 2E and 2F). To confirm further whether Cyp2e1-C2 includes the unique pericentral *GS*$^+$/*Lgr5*$^+$ hepatocyte subset, we sorted Lgr5-GFP$^+$ and Lgr5-GFP$^-$ hepatocytes from adult *Lgr5-rtTA-IRES-GFP* male mice and profiled their transcriptome by RNA-seq. Around 500 DEGs were identified in Lgr5-GFP$^+$ versus Lgr5-GFP$^-$ hepatocytes (Treat-FDR < 0.05; > 2-fold change). KEGG analysis revealed that pericentral genes/pathways enriched in the *Cyp2e1*$^+$ zone are also highly expressed in the Lgr5-GFP$^+$ subset (Figures S2A–S2C). Interestingly, a subset of the DEGs, including genes associated with the Wnt signaling pathway (Figure S2D), are exclusively expressed or silenced in *Lgr5*$^+$ but not in other hepatocytes within the *Cyp2e1*$^+$ zone. These findings collectively define *Lgr5*$^+$ cells as a distinct subpopulation of *Cyp2e1*$^+$ hepatocytes in this single-cell transcriptome profiling dataset (Figures S2E and S2F). We further integrated the gene expression signatures of the two major zones with the single-nucleus RNA-seq dataset of mouse liver tissues.[37] Remarkably, two distinct *Cyp2e1*$^+$ and *Gls2*$^+$ hepatocyte clusters were also readily detected, and an *Lgr5*$^+$/*Glul*$^+$/*Slc1a2*$^+$ subpopulation was further identified in the *Cyp2e1*$^+$ cluster (Figures S2G and S2H). Of note, the Gls2-C2 sub-cluster (Figure 2C) was not detected in this dataset. Moreover, a small subset of *Gls2*$^+$ hepatocytes could be found in the *Cyp2e1*$^+$ cluster in both datasets (Figures 2C and S2G).

Neonatal *Cyp2e1*$^+$ hepatocytes serve as the main cellular source for early liver mass expansion

To determine when pericentral and periportal zones are established during early development, liver sections from FVB wild-type mice at various postnatal stages were analyzed by immunofluorescence staining. We found that the pericentral expression pattern of Cyp2e1 was established as early as postnatal day (P)1, while Hal is weakly expressed around the periportal area at this stage (Figure S3A). From P7 onwards, the Cyp2e1$^+$ and Hal$^+$ zones were clearly defined (Figure S3A).

Figure 2. scRNA-seq data analysis identifying two major zonal hepatocyte populations in adult mouse livers

(A) Heatmaps showing the top 100 upregulated and downregulated DEGs in Tomato$^+$ (*Cyp2e1*$^+$) versus Tomato$^-$ (*Cyp2e1*$^-$) hepatocytes. The plot shows $\log_2$ counts per million, mean corrected and standardized for each gene. DEGs display a significant > 2-fold change (Treat-FDR < 0.05). $n = 3$ biological replicates per group.

(B) KEGG pathway enrichment analysis of DEGs between Tomato$^+$ versus Tomato$^-$ hepatocytes in (A).

(C) Uniform manifold approximation and projection (UMAP) plot of distinct hepatocyte populations in the single-cell RNA-seq (scRNA-seq) data from Su et al.[35] The DEGs from bulk RNA-seq data of *Cyp2e1*$^+$ versus *Cyp2e1*$^-$ (i.e., *Gls2*$^+$) hepatocytes in (A) were used as anchor genes for the integration analysis to generate the UMAP plot.

(D) Dot plot of the top 15 marker genes for *Cyp2e1*$^+$ and *Gls2*$^+$ hepatocytes. *Cyp2e1-C1* and *Cyp2e1-C2* clusters are merged into one *Cyp2e1*$^+$ population. *Gls2-C1* and *Gls2-C2* clusters are merged into one *Gls2*$^+$ population.

(E and F) Violin plots (E) and UMAP plots (F) showing expressions of indicated marker genes for different clusters in the scRNA-seq data.

The liver undergoes a significant increase in mass from birth to adulthood, with an ~12-fold increase between P1 and P42 (Figure S3B). We have previously reported that *Lgr5*$^+$ hepatocytes are primarily self-maintained from P7 onwards.[27] To trace the contribution of the wider population of pericentral hepatocytes to the generation of liver mass during homeostasis at different developmental stages, we pulsed *Cyp2e1/TetO-Cre/R26-Tomato* mice with DOX at neonatal (P7), adolescence (P21) and adulthood (7–8 weeks old) stages, and chased for various durations. Of note, adult mice were normally pulsed with DOX food and water for a week to achieve high labeling efficiency for lineage tracing. However, given the rapid expansion of the liver during the neonatal stage, a rapid and short administration of DOX is required. Thus, pups at P7 and P21 were pulsed with 1× intraperitoneal (i.p.) injection of DOX. Remarkably, *Cyp2e1/TetO-Cre/R26-Tomato* mice pulsed at P7 and analyzed after 3 weeks and 8 months of tracing exhibited a dramatic increase in the Tomato$^+$ cell population from 60% to 90% (Figures 3A and B). Likewise, the Tomato$^+$/Hal$^+$ double positive (DP) population increased from 20% to 60%. Importantly, the Hal$^+$ population also significantly increased in 8- to 9-month-old mice compared to P7 pups. On the other hand, *Gls2/TetO-Cre/R26-Tomato* pups pulsed with 1× i.p. injection of DOX at P7 showed a significant reduction in Tomato$^+$ population in the liver from 50% to 35% when traced for 8 months, while the Cyp2e1$^+$Tomato$^+$ DP population also showed a drastic decrease from 20% to less than 1% (Figures 3C and 3D). The expansion of the Tomato$^+$ population was also evident in the livers of *Cyp2e1/TetO-Cre/R26-Tomato* mice pulsed at P21 but with slower kinetics (Figures S3C and S3D). Liver sections analyzed after 3 weeks of tracing showed a slight expansion of Tomato$^+$ area. By 8 months, the Tomato$^+$ area increased to 80%, compared to 60% at 24 h after DOX induction. Moreover, the Tomato$^+$Hal$^+$ DP population also expanded 2-fold from 20% to 40%. The Hal$^+$ population also significantly increased in 8- to 9-month-old mice compared to P21 pups. Of note, *Cyp2e1/TetO-Cre/R26-Tomato* mice pulsed at P21 using a different method, i.e., via food and drinking water containing DOX, exhibited similar significant increases in their percentages of Tomato$^+$ area when analyzed immediately after DOX treatment compared to after 12 months of tracing (Figures S3E and S3F), while *Gls2/TetO-Cre/R26-Tomato* mice pulsed at P21 using the same method exhibited a slight but statistically insignificant decrease in Tomato$^+$ population (Figures S3G and S3H).

Collectively, the data from the two lineage-tracing models together indicate that a significant portion of the Hal$^+$ periportal zone was derived from *Cyp2e1*$^+$*Hal*$^+$ DP hepatocytes during early development with rapid growth of liver, while a subset of Hal$^+$ hepatocytes most adjacent to the portal vein are long lived and able to self-maintain.

Self-maintenance of *Cyp2e1*$^+$ and *Gls2*$^+$ zones during homeostasis and regeneration upon PH

We next sought to address the contribution of *Cyp2e1*$^+$ and *Gls2*$^+$ hepatocytes to adult liver homeostasis. The expansion of adult *Cyp2e1*$^+$ hepatocytes to the *Hal*$^+$ zone was not detectable after 3 months of tracing. By 8 months, the Tomato$^+$Hal$^+$ DP population seemed to increase from 10% to 20%, although it was not statistically significant. The total Tomato$^+$ population derived from *Cyp2e1*$^+$ hepatocytes also only showed a marginal increase that is statistically insignificant (Figures 3E and 3F). These results imply that the majority of hepatocytes in the *Gls2*$^+$ zone are not replaced by cells derived from pre-existing *Cyp2e1*$^+$ hepatocytes. In line with this, the Tomato$^+$ population remained unchanged in *Gls2/TetO-Cre/R26-Tomato* mice pulsed at adulthood over a tracing period of 8 months (Figures 3G and 3H), as well as in *Msfd2a-CreER/R26-Tomato* mice traces for 12 months (Figures S3I and S3J).

The remarkable regenerative capacity of the liver is evidenced by the rapid and efficient restoration of liver mass in adult mice within a few days after 2/3 PH.[38] We performed PH on *Cyp2e1/TetO-Cre/R26-Tomato* and *Gls2/TetO-Cre/R26-Tomato* mice to investigate the contribution of *Cyp2e1*$^+$ and *Gls2*$^+$ hepatocytes to acute liver regeneration. Adult mice were pulsed with DOX to induce Tomato expression in hepatocytes in the respective regions 1 week prior to surgery (Figure S4A). Liver lobes resected during the surgery were collected and analyzed in comparison to regenerated liver lobes collected at 14 days post-surgery, when the regeneration process has completed. We observed that the distribution pattern and percentage of Tomato$^+$ hepatocytes remain unchanged in liver sections before and after PH in both models (Figures S4B–S4D), suggesting that *Cyp2e1*$^+$ and *Gls2*$^+$ hepatocytes mainly regenerated their own lineages upon PH.

Gls2$^+$ hepatocytes repopulate the liver lobule upon chemical-induced pericentral injuries

We have previously reported that *Lgr5*$^+$ hepatocytes can be replenished by *Lgr5*$^-$ cells in adult livers upon pericentral injury induced by carbon tetrachloride (CCl_4).[27] To further investigate the contribution of *Cyp2e1*$^+$ and *Gls2*$^+$ hepatocytes to regeneration upon CCl_4 injury, adult *Cyp2e1/TetO-Cre/R26-Tomato* and *Gls2/TetO-Cre/R26-Tomato* mice were pulsed with DOX and subjected to 10 doses of CCl_4 over 3 weeks[39] (Figure 4A). Livers were harvested at three time points—immediately, 2 weeks, and 8 weeks after the last CCl_4 dose. The vast majority of Tomato$^+$ hepatocytes in the livers of *Cyp2e1/TetO-Cre/R26-Tomato* mice were depleted after CCl_4 treatment compared to vehicle controls (Figures 4B and 4C). Interestingly, while some sparse Tomato$^+$ hepatocytes survived the damage, they did not expand and form colonies even after 8 weeks. On the contrary, we observed a gradual expansion of the Tomato$^+$ population to the *Cyp2e1*$^+$ zone in the *Gls2/TetO-Cre/R26-Tomato* model (Figures 4D and 4E). Almost the entire liver lobule (~90%) was repopulated by Tomato$^+$ hepatocytes, and most *Cyp2e1*$^+$ cells were newly generated by pre-existing *Gls2*$^+$ hepatocytes even as early as 2 weeks after the last CCl_4 injection.

We also traced *Cyp2e1*$^+$ and *Gls2*$^+$ hepatocytes in the event of diethylnitrosamine (DEN)-induced pericentral damage. We administered 1 dose of DEN per week for 3 consecutive weeks to adult *Cyp2e1/TetO-Cre/R26-Tomato* and *Gls2/TetO-Cre/R26-Tomato* mice, starting 1 week after DOX pulsing (Figure 4F). More Tomato$^+$ hepatocytes survived DEN-induced damage in the *Cyp2e1/TetO-Cre/R26-Tomato* model compared to CCl_4-induced damage (Figures 4G and 4H). Interestingly, these Tomato$^+$ cells also did not expand to replenish the pericentral

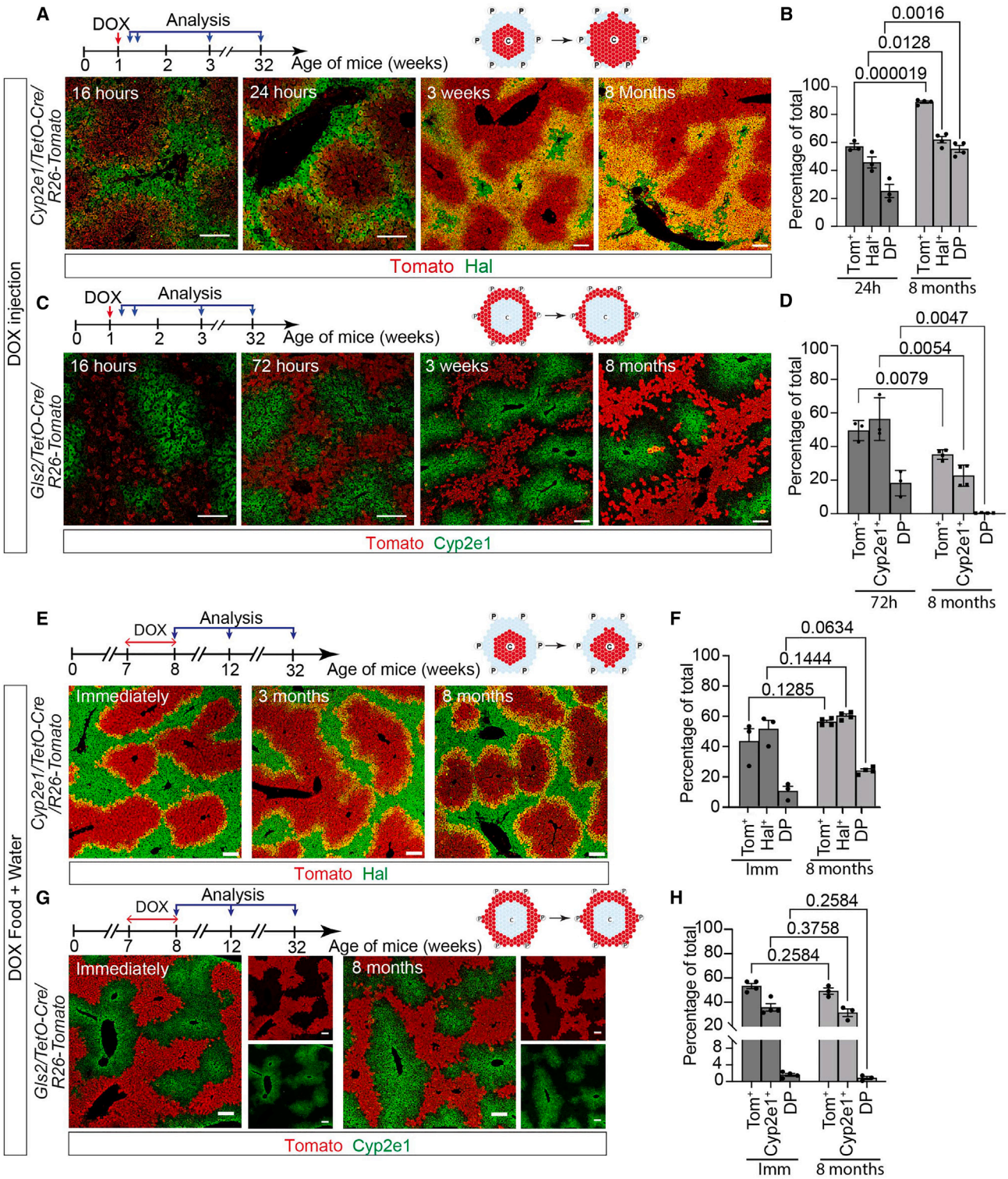

Figure 3. Neonatal liver growth is fueled by *Cyp2e1*$^+$ hepatocytes, but adult zonal hepatocytes are self-maintained

Representative confocal images of liver sections and quantitative analysis of the Tomato$^+$ population of *Cyp2e1/TetO-Cre/R26-Tomato* (A and B) and *Gls2/TetO-Cre/R26-Tomato* mice (C and D) pulsed at P7 and *Cyp2e1/TetO-Cre/R26-Tomato* (E and F) and *Gls2/TetO-Cre/R26-Tomato* (G and H) mice pulsed at adulthood. Error bars represent mean ± SEM. $n = 3$–4 mice per group. An average of 5,000 cells per site, 3–10 sites from the liver of each mouse were counted. $p < 0.05$ was calculated using multiple t test. Scale bars: (A, C, E, and G) 100 μm.

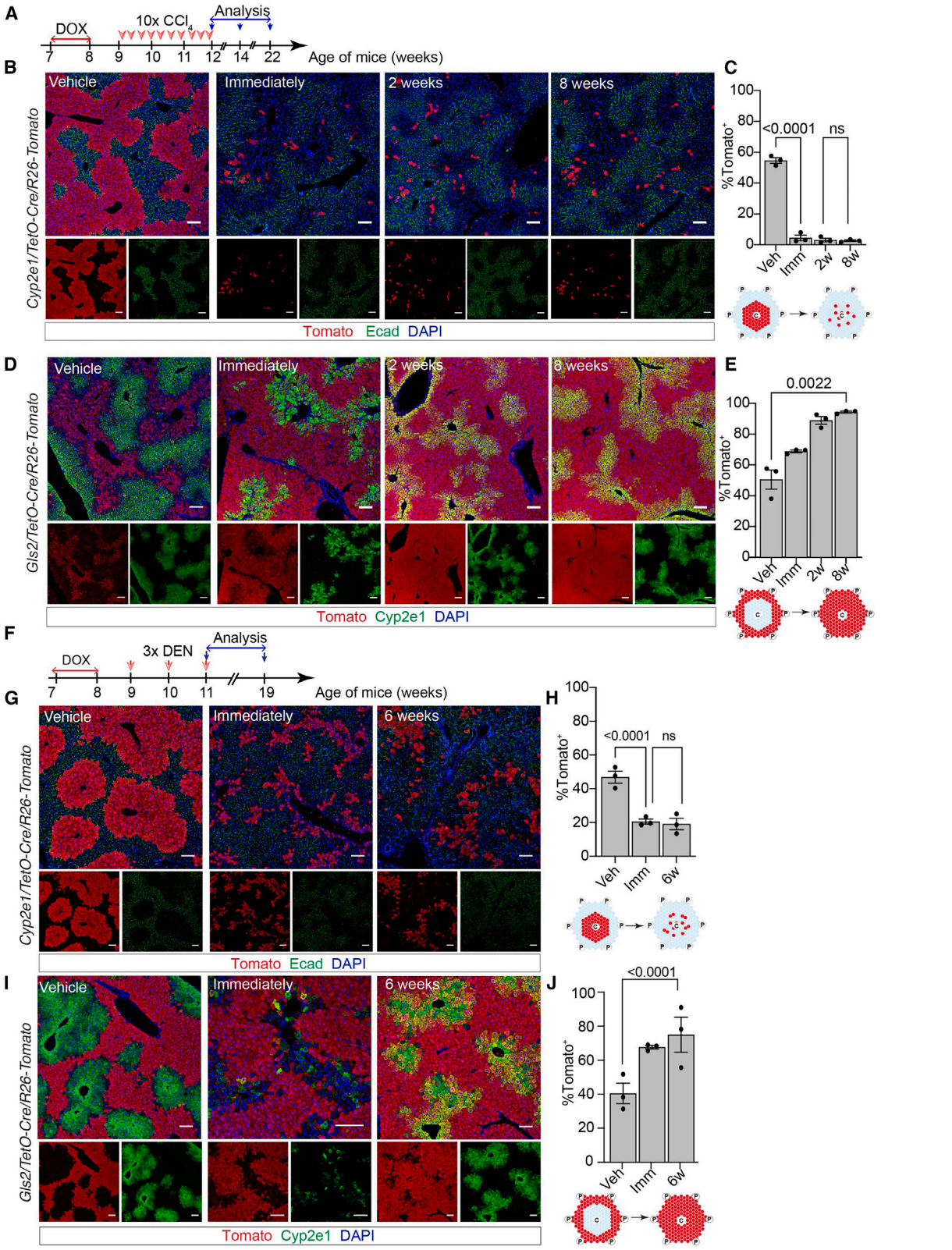

(legend on next page)

area after 8 weeks of tracing. DEN treatment in *Gls2/TetO-Cre/R26-Tomato* mice revealed the opposite results, in which the Cyp2e1$^+$ pericentral region was re-established within 6 weeks, with a significant expansion of the periportal Tomato$^+$ population from 40% to > 80% (Figures 4I and 4J).

Overall, these results suggest that in the event of chemical-induced pericentral injuries, the periportal *Gls2*$^+$ population is the main cell source for replenishment of the damaged pericentral hepatocytes.

Cyp2e1$^+$ hepatocytes are rapidly replenished by other cells upon depletion by DTA

The *Ccnd1* gene that encodes Cyclin D1 protein was used as a genetic marker to label midlobular hepatocytes in a previous study.[28] Our bulk RNA-seq data revealed that *Ccnd1* expression is ~8 times higher in the *Cyp2e1*$^+$ zone compared to the *Cyp2e1*$^-$ zone (Figure 5A). Indeed, approximately 80% of cyclin D1$^+$ hepatocytes are situated within the Tomato$^+$ zone in the liver of adult *Cyp2e1/TetO-Cre/R26-Tomato* mice, and they are more enriched in the area distant from the central vein (Figure 5B). To further examine whether the *Cyp2e1*$^+$ population, which contains most of the *Ccnd1*$^+$ cells, is indispensable for liver regeneration, we crossed *Cyp2e1/TetO-Cre/R26-Tomato* mice with Rosa26-diphtheria toxin subunit A (DTA) mice to generate the *Cyp2e1/TetO-Cre/R26-DTA/R26-Tomato* line for rapid depletion of *Cyp2e1*$^+$ hepatocytes (Figure 5C). Adult *Cyp2e1/TetO-Cre/Tomato* mice with or without the DTA allele were administered DOX for 3 days (Figure 5D). Very few Tomato$^+$ and *Cyp2e1*$^+$ cells were detected in the livers of *Cyp2e1/TetO-Cre/R26-DTA/R26-Tomato* mice (Figure 5E). Moreover, GS$^+$ cells were also thoroughly depleted (Figure S5B), while the Hal$^+$ zone remained unchanged (Figure S5B). These results indicated the specific and robust depletion of *Cyp2e1*$^+$ hepatocytes by DTA. By 2 weeks of the regenerative phase, the Cyp2e1$^+$ and GS$^+$ zones were completely restored, while the Tomato$^+$ population remained scarce (Figures 5F, S5C, and S5D). Of note, Tomato was efficiently turned on in almost all Cyp2e1$^+$ hepatocytes in the livers of control *Cyp2e1/TetO-Cre/Tomato* mice under this DOX treatment condition (Figures 5G and S5A). The body weights of *Cyp2e1/TetO-Cre/R26-DTA/R26-Tomato* mice rapidly decreased by up to 10% during the 3 days of DOX treatment and recovered within 1 day after DOX treatment was stopped (Figure 5H). Collectively, these data suggest that DTA-depleted *Cyp2e1*$^+$ hepatocytes were rapidly replaced by cells derived from the *Cyp2e1*$^-$ hepatocytes to restore the metabolic functions of the *Cyp2e1*$^+$ zone.

Ccnd1$^+$ hepatocytes do not serve as the main cell source in regeneration upon PH and severe CCl_4-induced damage

To address the role of *Ccnd1*$^+$ hepatocytes in liver regeneration, we generated a new DOX-inducible knockin mouse strain, *Ccnd1-EGFP-P2A-rtTA3*, by replacing the stop codon of the *Ccnd1* gene with a *EGFP-P2A-rtTA3* cassette. This strain expresses the Cyclin D1-GFP fusion protein and rtTA protein separately from the same mRNA under the control of the endogenous *Ccnd1* protomer. We crossed *Ccnd1-EGFP-P2A-rtTA3* mice to *TetO-Cre* and *Rosa26-Tomato* mice to generate the *Ccnd1/TetO-Cre/R26-Tomato* model for lineage tracing (Figure S6A). Adult *Ccnd1/TetO-Cre/R26-Tomato* mice were treated with DOX for 1 week to induce Tomato expression. Tomato$^+$ cells are mainly located at the edge of the Cyp2e1$^+$ zone in liver sections of *Ccnd1/TetO-Cre/R26-Tomato* mice harvested 1 week after DOX treatment (Figure S6B), which is consistent with our data obtained from co-staining of Tomato and Cyclin D1 in liver sections of *Cyp2e1/TetO-Cre/R26-Tomato* mice (Figure 5B). We next sought to determine the contribution of *Ccnd1*$^+$ hepatocytes in the liver of adult *Ccnd1/TetO-Cre/R26-Tomato* mice upon PH (Figures S6C–S6E). There was an increase in the Tomato$^+$ population in both the Cyp2e1$^+$ and Hal$^+$ zones of the regenerated lobes compared to the resected lobes. However, we did not identify lobular areas that are dominantly constituted of Tomato$^+$ cells. Collectively, our data suggest that *Ccnd1*$^+$ hepatocytes are unlikely the main cell source for liver regeneration upon PH.

To determine the contribution of *Ccnd1*$^+$ hepatocytes in liver regeneration upon pericentral liver damage, adult mice were pulsed with DOX and treated with 1× CCl_4 (Figure S6F). Livers were harvested at 24 h and 2 weeks after the injection. Co-staining of liver sections with Tomato, Hal, and GS revealed an increase in the Tomato$^+$ population in the livers with a 2 week recovery period after CCl_4 injection compared to vehicle control, suggesting that *Ccnd1*$^+$ hepatocytes in proximity to the damaged pericentral area had expanded to replenish those lost (Figures S6G and S6H). To further decipher the roles of *Ccnd1*$^+$ hepatocytes in prolonged pericentral damage, *Ccnd1/TetO-Cre/R26-Tomato* mice were subjected to 10× CCl_4 over 3 weeks (Figure S6I). Livers were harvested immediately after the last dose of CCl_4 as well as 2 weeks after the last dose of CCl_4. Co-staining of liver sections with Tomato, Hal, and GS revealed a striking reduction in the number of Tomato$^+$ cells in livers harvested immediately after CCl_4 treatment compared to vehicle controls (Figures S6J and S6K). Although a minute number of Tomato$^+$ cells could survive the injury, these cells did not

Figure 4. Periportal *Gls2*$^+$ hepatocytes replenish the pericentral zone upon acute pericentral injuries

(A) Schematic illustration of experimental strategy for CCl_4-induced liver injury.

(B–E) Representative confocal images of liver sections and quantitative analysis of the Tomato$^+$ population in livers of *Cyp2e1/TetO-Cre/R26-Tomato* (B and C) and *Gls2/TetO-Cre/R26-Tomato* (D and E) mice harvested immediately (Imm), 2 weeks, or 8 weeks after the last dose of CCl_4 treatment or untreated control mice.

(F) Experimental strategy for DEN-induced pericentral liver injury.

(G–J) Representative confocal images and quantitative analysis of the Tomato$^+$ population of livers from *Cyp2e1/TetO-Cre/R26-Tomato* (G and H) and *Gls2/TetO-Cre/R26-Tomato* (I and J) mice. Livers were harvested from mice Imm or 6 weeks after the last dose of DEN administration or untreated control mice. Error bars represent mean ± SEM. $n = 3$ mice per group. An average of 4,000 cells per site, 3–10 sites from the liver of each mouse were counted. $p < 0.05$ was calculated using multiple t test.

Scale bars: (B, D, G, and I) 100 μm.

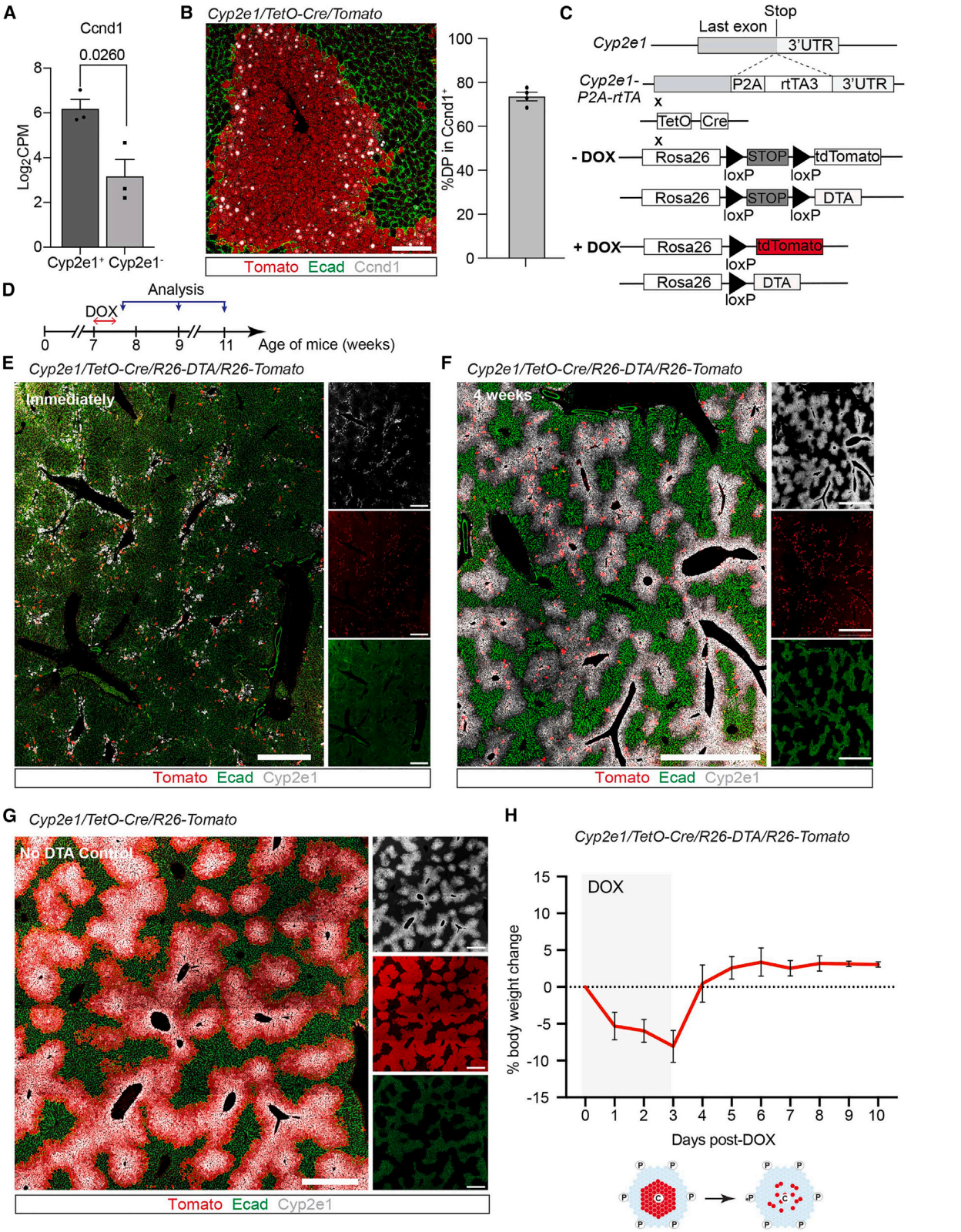

(legend on next page)

expand to replenish the damaged lobular areas, as was evident in the livers of mice with a 2 week recovery period after CCl_4 treatment (Figures S6J and S6K). Our data unveil that although pre-existing *Ccnd1*$^+$ cells in the liver may be activated to replace damaged pericentral cells in the event of minor damage, they are vulnerable to prolonged CCl_4-induced damage and do not serve as the main cell source for liver regeneration in severe CCl_4-induced pericentral damage.

Cyp2e1$^+$ hepatocytes contribute significantly to regeneration of the periportal zone upon DDC-induced injury

We next sought to determine whether pericentral hepatocytes are capable of repopulating periportal hepatocytes upon periportal injury. A 3,5-diethoxycarbonyl-1,4-dihydrocollidine (DDC) diet is known to induce chronic liver damage and ductular reactions that resemble cholangiopathies in human by increasing biliary porphyrin in the periportal region of the liver lobule.[39] After pulsing them with DOX, we fed adult *Cyp2e1/TetO-Cre/R26-Tomato* and *Gls2/TetO-Cre/R26-Tomato* mice with a diet containing 0.1% DDC over short-term (6 weeks) and long-term (5 months) durations (Figure 6A). The Tomato$^+$ population evidently expanded in *Cyp2e1/TetO-Cre/R26-Tomato* livers compared to untreated controls, following both short-term and long-term DDC treatment (Figure 6B). A 50%–70% expansion of the Tomato$^+$ population was observed after short-term treatment for 6 weeks (Figure 6C). In some areas, the entire lobule was constituted by only Tomato$^+$ hepatocytes. Long-term DDC treatment for 5 months and recovery of the liver thereafter did not cause further expansion of the Tomato$^+$ population (Figures 6B, 6C, and S7A). Interestingly, although a majority of the liver lobule was repopulated by Tomato$^+$ cells originating from the pre-existing pericentral *Cyp2e1*$^+$ population, a significant proportion of periportal hepatocytes (*Hal*$^+$ and Tomato$^-$) were able to survive (Figure 6B).

On the other hand, we observed a massive depletion of Tomato$^+$ cells in *Gls2/TetO-Cre/R26-Tomato* livers from approximately 50% to 15% after 6 weeks of DDC treatment compared to controls (Figures 6D and 6E). Prolonged DDC treatment did not further deplete the periportal Tomato$^+$ cells. Interestingly, liver sections from mice treated with DDC for 5 months showed formation of large Tomato$^+$ colonies, suggesting that a portion of pre-existing periportal Tomato$^+$ cells likely gained resistance to DDC damage and were able to proliferate to replenish the nearby damaged *Gls2*$^+$ hepatocytes (Figure S7B). After 4 months of recovery, we observed an increase in the Tomato$^+$ population (Figure 6E). A similar phenomenon was observed in lineage tracing of TAM-inducible *Msfd2a-CreER/R26-Tomato* mice upon DDC damage (Figure S7C). To further confirm the clonal formation and expansion by surviving periportal hepatocytes upon DDC damage, we treated adult *Gls2/TetO-Cre/R26-Tomato* mice with 1× i.p. injection of DOX at 0.5 mg/mouse to induce low labeling of *Gls2*$^+$ hepatocytes. Consistent with our previous findings, we observed the formation of Tomato$^+$ colonies in some lobules after the mice were treated with DDC for 5 months (Figure S7D).

Taken together, our results on the regeneration of pre-existing *Cyp2e1*$^+$ and *Gls2*$^+$/*Msfd2a*$^+$ hepatocytes showed that periportal and pericentral hepatocytes harbor high levels of plasticity and regenerate efficiently upon chronic periportal liver damage induced by DDC.

Lgr5$^+$ hepatocytes serve as an important cell source for liver repair upon DDC-induced injury

The results above showed that *Cyp2e1*$^+$ hepatocytes contribute significantly to liver regeneration upon periportal injury induced by DDC. As the *Lgr5*$^+$/*GS*$^+$ subset is located closest to the central veins within the *Cyp2e1*$^+$ zone, we next investigated the role of *Lgr5*$^+$/*GS*$^+$ cells in this liver regeneration process. Notably, unlike our Lgr5-rtTA model,[27] the lineage-tracing models for *GS*$^+$ hepatocytes in the two previous studies showed profound leakiness in the absence of TAM,[29,30] which suggests that those models are not suitable for lineage-tracing experiments. After pulsing them with DOX, we subjected adult *Lgr5-rtTA/TetO-Cre/R26-Tomato* mice to DDC diet for a short term of 6 weeks or a long term of 5 months (Figure 7A). Significant expansion of the Tomato$^+$ population was observed when livers were analyzed immediately after 6 weeks of DDC treatment. Interestingly, the expansion was restricted to the pericentral *Cyp2e1*$^+$ zone in most lobules (Figure 7C). When the mice were left to recover for 6 months after 6 week DDC treatment, we observed a Tomato$^+$Hal$^+$ DP population in the liver, indicating the further expansion of cells derived from *Lgr5*$^+$ hepatocytes into the periportal zone to replenish the damaged periportal hepatocytes during recovery (Figure 7D). The profound expansion of hepatocytes derived from the pre-existing *Lgr5*$^+$ cells to the periportal *Hal*$^+$ zone was observed in livers after 6 months of recovery following 5 months of DDC treatment (Figure 7E), in which the Tomato$^+$ population increased from less than 10% before treatment to ~50% on average and up to 80% in some lobules (Figure 7F). Similar expansion dynamics of the Tomato$^+$ population was also evident in the TAM-inducible *Lgr5-T2A-CreERT2/R26-Tomato* knockin mouse model (Figures S8B and S8C). Interestingly, when *Lgr5-rtTA/TetO-Cre/R26-Tomato* mice

Figure 5. Rapid restoration of *Cyp2e1*$^+$ hepatocytes by other hepatocytes upon DTA-induced depletion

(A) Bar graph showing expression levels of *Ccnd1* in *Cyp2e1*$^+$ versus *Cyp2e1*$^-$ hepatocyte populations in bulk RNA-seq analysis.

(B) Representative confocal images and quantitative analysis of Cyclin D1$^+$ cells in liver sections of *Cyp2e1/TetO-Cre/R26-Tomato* mice pulsed with DOX. Bar graph showing the percentage of cells expressing both Tomato and Cyclin D1 (DP) in total Cyclin D1$^+$ cells.

(C) Schematic illustration of the mouse model for acute deletion of *Cyp2e1*$^+$ hepatocytes by DTA expression.

(D) Experimental design for simultaneous induction of DTA and Tomato expressions in *Cyp2e1/TetO-Cre/R26-DTA/R26-Tomato* mice.

(E–G) Representative confocal images of liver sections from *Cyp2e1/TetO-Cre/R26-DTA/R26-Tomato* mice harvested immediately (E) or 4 weeks (F) after 3 day DOX treatment. *Cyp2e1/TetO-Cre/Tomato* mice without the DTA knockin allele were harvested immediately after 3 day DOX treatment as controls (G).

(H) Graph showing percentage of body weight changes in *Cyp2e1/TetO-Cre/R26-DTA/R26-Tomato* mice during 3-day DOX treatment (days 0–3) and in the week following treatment (days 4–10). Error bars represent mean ± SEM. $n = 3$ mice per group. $p < 0.05$ was calculated using multiple t test.

Scale bars: (B) 100 μm and (E–G) 500 μm.

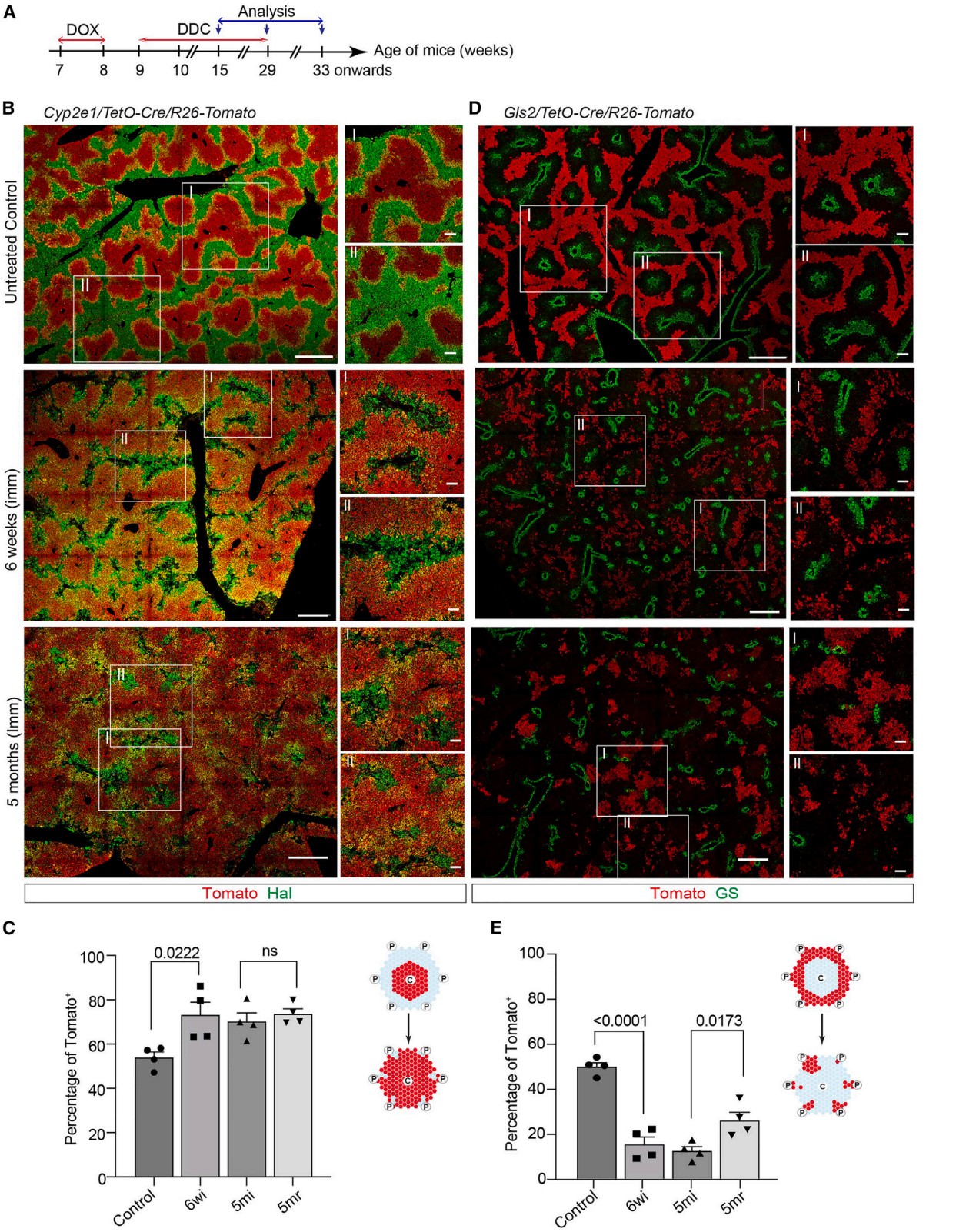

(legend on next page)

were treated with DDC for only 2 weeks, we found that the expansion of *Lgr5*-descendant hepatocytes barely reached the periportal *Hal*$^+$ zone even when the mice were left to recover for up to 18 months, suggesting that *Lgr5*$^+$ cells are activated at the early stage of DDC damage and that the repair process is halted once the damaged area has been fully recovered (Figures S8D and S8E).

To examine the distribution and pattern of hepatocyte proliferation during liver regeneration upon DDC damage, we conducted sequential labeling of BrdU and EdU. *Lgr5-rtTA/TetO-Cre/R26-Tomato* mice were on DDC diet for 3 weeks, followed by 1 week of recovery (Figure 7G). In the first 2 weeks, mice were given drinking water containing BrdU for 2 cycles of 5 day pulses, with a 2 day interval between each cycle. In the last week of DDC treatment and before a subsequent week of recovery, mice were provided with drinking water containing EdU for 2 cycles of 5 day pulses, with a 2 day interval between each cycle (Figure 7G). As such, cells that were proliferating in the first 2 weeks of DDC treatment were labeled with BrdU, while cells that proliferated subsequently were labeled with EdU. The Tomato$^+$ population derived from *Lgr5*$^+$ hepatocytes was significantly expanded from 20% to 50% of the *Cyp2e1*$^+$ pericentral region after 3 weeks of DDC treatment compared to in the untreated controls (Figure 7I). Interestingly, ~4 times more BrdU$^+$ or EdU$^+$ cells were found in the *Cyp2e1*$^-$ zone. This likely implies that the nearby healthy hepatocytes were preferentially stimulated by proliferation signals from periportal injured hepatocytes to enter the cell cycle in this chronic liver damage model (Figure 7J). Moreover, a portion of Tomato$^+$ hepatocytes that were no longer located in the *Lgr5*$^+$/*GS*$^+$ layers were BrdU and EdU double positive (indicated by white arrowheads), suggesting that these Lgr5-descendant cells have divided at least twice during regeneration, with the later division occurring after they had moved out from the *Lgr5*$^+$/*GS*$^+$ zone (Figures 7I and 7H).

DISCUSSION

Functional zonation is a key feature of the liver lobule structure. Our immunofluorescence co-staining study using pericentral and periportal markers showed that the liver lobule is constituted by two main zones—pericentral and periportal—with limited overlap between them. We developed mouse models to facilitate the efficient isolation of these two major zonal hepatocyte subsets at high purity for molecular characterization and tracing. Bulk RNA-seq data revealed that these two zonal hepatocytes show distinct gene expression signatures. Remarkably, integration analysis of hepatocytes from publicly available single-cell RNA-seq data[36] and single-nucleus RNA-seq data[37] on a large number of cells using these gene signatures revealed that hepatocytes are classified into two molecular clusters, namely periportal *Gls2*$^+$ and pericentral *Cyp2e1*$^+$ populations. Although a minute proportion of hepatocytes expressing both *Gls2* and *Cyp2e1* were detected in single-cell or single-nucleus profiling, most of these cells were clustered into the *Cyp2e1*$^+$*Lgr5*$^-$ population. Overall, these findings demonstrate that the liver lobule can be functionally divided into the pericentral and periportal zones, which are typically marked by the expression of *Cyp2e1 and Gls2/Ecad/Hal*, respectively. Hence, to refine the typical three-zone model, other than zone 1 marked by *Gls2/Ecad/Hal*, hepatocytes among the *Cyp2e1*$^+$ population can be further divided into two spatial and molecular zones—they are positive for Cyp2e1 but either positive (zone 3) or negative (zone 2) for Lgr5/GS. It is also important to note that hepatocytes in each zone likely maintain a certain degree of heterogeneity, and the liver lobule may be organized in a gradient manner for certain functions. Consistent with our RNA-seq results, data from single-nucleus multi-omics, including assay for transposase-accessible chromatin using sequencing (ATAC-seq) and RNA-seq, also supported that the liver lobule can be divided into three major regulatory topics—two of them correspond to the *Lgr5*$^+$ and *Lgr5*$^-$ subpopulations of the *Cyp2e1*$^+$ hepatocytes and the third one corresponds to the *Gls2*$^+$ hepatocyte populations (Figures 2C and S2G). Furthermore, we showed that the *Cyp2e1*$^+$ and *Gls2*$^+$ zones are highly enriched in the transcription repressors Tcf7l1 and Tbx3, respectively. This finding is in line with an earlier study that identified these two repressors as key regulators of liver zonation.[37] Moreover, we also found that another key transcription factor of Wnt signaling, Tcf7, is highly enriched in *Cyp2e1*$^+$ hepatocytes. However, the role of this protein in the transcriptional regulation of the two major zones remains unclear and needs to be addressed in future studies.

The contribution of different zonal hepatocyte subsets to the generation of new hepatocytes during adult liver homeostasis and regeneration has been a matter of debate. The high labeling efficiencies and combined use of our lineage-tracing models for pericentral *Cyp2e1*$^+$ and periportal *Gls2*$^+$ hepatocytes enabled us to investigate the cell fate of almost all hepatocytes. In contrast to the findings from previous studies, long-term lineage tracing of *Cyp2e1*$^+$ hepatocytes in adult mice showed little expansion of the Tomato$^+$ population in our *Cyp2e1/TetO-Cre/R26-Tomato* model.[29] Accordingly, we found the *Gls2*$^+$/*Msfd2a*$^+$ hepatocytes are long lived and self-maintained during adult homeostasis. Interestingly, we found a small subset of cells expressing both *Cyp2e1* and *Gls2* between the two main zones in the analysis of single-cell profiling data (Figure S2G) and lineage tracing of the *Cyp2e1/TetO-Cre/R26-Tomato* model (Figure 3E). This subset of cells do not seem to play a preferential regeneration role during long-term homeostasis. We also examined how the two major zonal hepatocytes are replenished during rapid liver regeneration upon PH and found that both

Figure 6. Pericentral *Cyp2e1*$^+$ hepatocytes contribute significantly to regeneration upon chronic periportal injury

(A) Experimental strategy for DDC-induced liver injury.

(B–E) Representative confocal images of liver sections and quantitative analysis of the Tomato$^+$ population of *Cyp2e1/TetO-Cre/R26-Tomato* (B and C) and *Gls2/TetO-Cre/R26-Tomato* (D and E) mice. Livers were harvested from mice immediately after 6 weeks (6 weeks [Imm]; 6wi) or 5 months (5 months [Imm]; 5mi) of DDC treatment or after up to 4 months of recovery post-5 months of DDC treatment (5mr) or from untreated control mice. Error bars represent mean ± SEM. $n = 4$ mice per group. An average of 4,000 cells per site, 3–10 sites from the liver of each mouse were counted. $p < 0.05$ was calculated using multiple t test.

Scale bars: (B and D) 500 μm (left) and 100 μm (right).

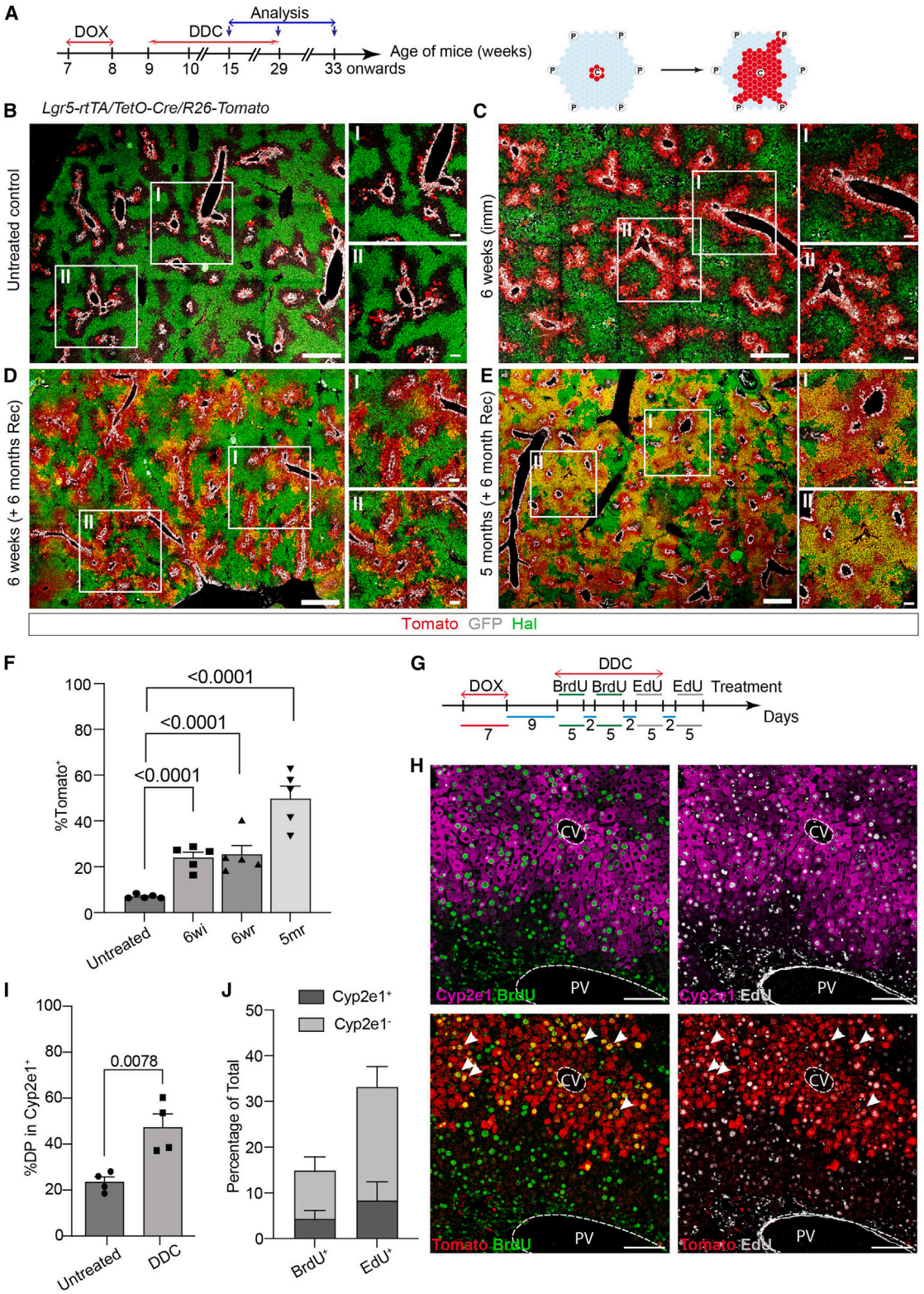

(legend on next page)

hepatocyte populations favor a self-maintenance mode. Notably, the *Lgr5*$^+$ population also appears to persist throughout their lifespan and does not contribute to the generation of hepatocytes in other lobular zones during homeostasis.[27,40]

Since mammalian epithelial cells have been shown to undergo cell fate changes during development in other tissues, we intended to inspect possible cell fate changes that may happen during neonatal development of the liver. We found that the pericentral *Cyp2e1*$^+$ zone is defined as early as P1. Lineage-tracing analysis on the *Cyp2e1/TetO-Cre/R26-Tomato* model showed that pericentral *Cyp2e1*$^+$ hepatocytes serve as the main reservoir for the generation of new hepatocytes during the massive growth of liver mass. Interestingly, the combined data from the *Cyp2e1 and Gls2* models suggests that *Cyp2e1*$^+$*Hal*$^+$ DP hepatocytes only expand toward the *Hal*$^+$ periportal cells during early liver development. However, the role of this unique hepatocyte subset needs further investigation in a mouse model where these cells can be specifically labeled and traced. Interestingly, lineage tracing of *Lgr5*$^+$ cells revealed that they maintained their own lineage throughout their lifetime from neonatal development to adult homeostasis and PH,[27] suggesting that the cell fate of *Lgr5*$^+$ hepatocytes is established and restricted at early developmental stages. Taken together, our data uncover a wave of hepatocyte expansion from the pericentral *Cyp2e1*$^+$*Lgr5*$^-$ population toward the portal vein during neonatal maturation stages of the liver. Moreover, lineage tracing of neonatal and adult *Cyp2e1*$^+$ hepatocytes revealed a cell fate switch in these cells during development.

To examine the potential plasticity of zonal hepatocyte populations in adult livers, we subjected mice from different lineage-tracing models to distinct liver injuries. We found that the majority of pre-existing *Cyp2e1*$^+$ hepatocytes were depleted and replaced by new hepatocytes generated from *Gls2*$^+$ cells when mice were subjected to pericentral injuries by DEN or CCl_4. Interestingly, a recent study reported that a layer of *Cyp2e1*$^+$ hepatocytes next to the *Gls2*$^+$ zone were able to survive through a single dose of CCl_4 and subsequently served as the main cell source for replenishing damaged cells in the *Cyp2e1*$^+$ zone.[41] These data, together with our results, strongly suggest that a local or "self-repair" mode of the *Cyp2e1*$^+$ pericentral regeneration is favored when the damage is less severe and short lived. However, in the case of severe and prolonged damage, this self-recovery mechanism is lost, and other zonal hepatocytes take over the role of replenishing the damaged hepatocytes. Interestingly, we also observed a small number of pre-existing *Cyp2e1*$^+$ cells that could survive in the presence of DEN or CCl_4 treatment but were unable to proliferate and clonally expand. On the other hand, both self-repair of *Gls2*$^+$ cells as well as regeneration of new *Gls2*$^+$ hepatocytes by *Cyp2e1*$^+$ cells were found to simultaneously occur in different liver lobules in the periportal DDC liver injury model (Figure 6). Moreover, a massive expansion of the rare pericentral *Lgr5*$^+$ population most adjacent to the central vein in response to periportal liver injury caused by DDC treatment challenged the recent notion that midlobular *Ccnd1*$^+$ hepatocytes serve as the main cell source for generating new hepatocytes during liver regeneration upon zone-specific liver injuries.[29,30,42] Since the majority of *Ccnd1*$^+$ hepatocytes are situated within the *Cyp2e1*$^+$ zone, and DTA-mediated depletion of *Cyp2e1*$^+$ cells was shown to be rapidly restored by other cells, we posit that midlobular *Ccnd1*$^+$ hepatocytes are dispensable for liver regeneration. Lineage tracing of *Ccnd1*$^+$ hepatocytes (Figure S6) provides further support that this population of cells is not essential for liver regeneration, at least in the severe CCl_4-induced liver damage model.

In summary, we found that the two major zones marked by *Cyp2e1* and *Gls2* expression in the mouse liver lobule exhibit distinct gene expression signatures. Other than the typical zone 1 marked by *Gls2/Hal/Ecad*, the *Cyp2e1*$^+$ hepatocytes can be divided into zone 2 and zone 3 based on the expression of *Lgr5/GS*. While pericentral *Cyp2e1*$^+$ hepatocytes serve as the cell source for fueling massive liver growth during early neonatal development, hepatocytes in different zones mainly adapt to a self-maintaining mode during adult homeostasis. Local repair or self-recovery of hepatocytes is likely the preferred mechanism for liver regeneration upon diverse injuries. However, mature hepatocytes at different zonal locations across the liver lobule harbor high plasticity to give rise to other hepatocyte populations. The plasticity of zonal hepatocytes during liver regeneration is determined by the type, severity, and duration of liver injuries.

Limitations of the study

Our results from the *Cyp2e1-rtTA* lineage-tracing model suggest thin overlapping hepatocyte layers between the *Cyp2e1*$^+$ zone and the periportal *Gls2*$^+$ zone. Due to the lack of an appropriate mouse model to label and trace these *Cyp2e1*^{low}*Gls2*$^+$ hepatocytes, we have not specifically investigated their molecular features and their roles in liver development, homeostasis, and

Figure 7. *Lgr5*$^+$ hepatocytes expand to replenish pericentral and periportal zones upon DDC-induced liver injuries

(A) Schematic illustration of DDC-induced liver injury experiment performed on *Lgr5/TetO-Cre/R26-Tomato* mice.

(B–E) Representative confocal images of liver sections of untreated control mice (B) or mice analyzed immediately after 6 weeks of DDC treatment (C), after 6 months of recovery from 6 weeks of DDC treatment (D), or after 6 months of recovery from 5 months of DDC treatment (E).

(F) Bar graph showing the percentage of Tomato$^+$ population in livers of untreated controls versus livers harvested immediately after 6 weeks (6wi), after recovery from 6 weeks of DDC treatment (6wr), or after recovery from 5 months of DDC treatment (5mr).

(G) Experimental design for sequential BrdU and EdU labeling of hepatocytes upon DDC-induced liver injury in *Lgr5/TetO-Cre/R26-Tomato* mice.

(H) Representative confocal images of liver sections of *Lgr5/TetO-Cre/R26-Tomato* mice after BrdU and EdU labeling. White arrowheads highlighted several Tomato$^+$ hepatocytes that expressed both BrdU and EdU.

(I) Quantitative analysis of Tomato$^+$ hepatocytes within the *Cyp2e1*$^+$ population in livers from untreated and DDC-treated *Lgr5/TetO-Cre/R26-Tomato* mice. DP, Tomato$^+$Cyp2e1$^+$ cells.

(J) Quantitative analysis of cells expressing BrdU and EdU in *Cyp2e1*$^+$ and *Cyp2e1*$^-$ zones after DDC treatment. Error bars represent mean ± SEM. $n = 4–5$ mice per group. An average of 4,000 cells per site, 3–10 sites from the liver of each mouse were counted. $p < 0.05$ was calculated using multiple t test.

Scale bars: (B–E) 500 μm (left) and 100 μm (right) and (H) 100 μm.

regeneration. Although we provided compelling evidence suggesting that midlobular *Ccnd1*$^+$ hepatocytes are dispensable for regeneration upon severe pericentral liver injury, we did not examine the contributions of *Ccnd1*$^+$ hepatocytes in long-term homeostasis or periportal liver injuries. While we conclude that *Cyp2e1*$^+$ and *Gls2*$^+$ zonal populations can self-maintain, there is the possibility that certain subsets of cells in each of two major hepatocyte populations may harbor preferable regeneration ability.

RESOURCE AVAILABILITY

Lead contact

Further information and requests for resources and reagents should be directed to and will be fulfilled by the lead contact, Nai Yang Fu (fu@wehi.edu.au).

Materials availability

All reagents will be made available by the lead contact author after completion of a materials transfer agreement.

Data and code availability

- Data reported in this paper will be shared by the lead contact upon request.
- This paper does not report original code.
- Any additional information required to re-analyze the data reported in this paper is available from the lead contact upon request.

ACKNOWLEDGMENTS

We are grateful to Z.M. Lim and N.H.B. Hamadee for assistance with FACS analysis/sorting and histology. We thank Dr. M.M.D. Varela and H.L. Chung at SingHealth Animal Vivarium, K. Sacadevan at SingHealth Advanced Bioimaging, and S. Jagannathan for critical readings and valuable comments on the manuscript. This work was supported by NMRC OF-YIRG (MOH-000546), the Gilead Research Scholars Liver Disease Program (Asia) (2020-Gilead-001), NHMRC Ideas Grant (#2037907), and Khoo Bridge Funding Awards. N.Y.F. and C.H.A. were supported by Victorian Cancer Agency Mid-Career Research Fellowship (MCRF22013) and NMRC OF-YIRG (MOH-000935), respectively; G.K.S. was supported by an NHMRC Fellowship (#1058892) and Investigator Grant (#2025645); and Y.C. was supported by an MRFF Investigator Grant (#1176199).

AUTHOR CONTRIBUTIONS

N.Y.F. and C.H.A. designed the study. C.H.A., P.A., J.Y., F.G., Y.Y., and S.N. performed experiments. J.C., Y.C., L.W., and G.K.S. performed bioinformatic analysis of RNA-seq data. N.Y.F., C.H.A., J.L., P.K.H.K.H.C., and D.M.V. carried out interpretation of data. J.E.V., J.E.V., N.B., and D.L.S. provided critical reagents and analyzed relevant data. N.Y.F. and C.H.A. wrote the manuscript.

DECLARATION OF INTERESTS

The authors declare no competing interests.

STAR★METHODS

Detailed methods are provided in the online version of this paper and include the following:

- KEY RESOURCES TABLE
- EXPERIMENTAL MODEL AND STUDY PARTICIPANT DETAILS
- METHOD DETAILS
  - Doxycycline and tamoxifen administration
  - Liver injury models
  - Histology and immunofluorescence staining
  - BrdU and EdU administration
  - Western blot analysis
  - FACS sorting of hepatocytes and RNA-seq
  - RNA-seq data analysis
  - scRNA-seq data analysis
- QUANTIFICATION AND STATISTICAL ANALYSIS

SUPPLEMENTAL INFORMATION

Supplemental information can be found online at https://doi.org/10.1016/j.celrep.2024.115093.

Received: August 5, 2024
Revised: October 16, 2024
Accepted: November 29, 2024
Published: December 24, 2024

REFERENCES

1. Magami, Y., Azuma, T., Inokuchi, H., Kokuno, S., Moriyasu, F., Kawai, K., and Hattori, T. (2002). Cell proliferation and renewal of normal hepatocytes and bile duct cells in adult mouse liver. Liver *22*, 419–425. https://doi.org/10.1034/j.1600-0676.2002.01702.x.
2. MacDONALD, R.A. (1961). "Lifespan" of Liver Cells: Autoradiographic Study Using Tritiated Thymidine in Normal, Cirrhotic, and Partially Hepatectomized Rats. Arch. Intern. Med. *107*, 335–343. https://doi.org/10.1001/archinte.1961.03620030023003.
3. Kopp, J.L., Grompe, M., and Sander, M. (2016). Stem cells versus plasticity in liver and pancreas regeneration. Nat. Cell Biol. *18*, 238–245. https://doi.org/10.1038/ncb3309.
4. Miyajima, A., Tanaka, M., and Itoh, T. (2014). Stem/progenitor cells in liver development, homeostasis, regeneration, and reprogramming. Cell Stem Cell *14*, 561–574. https://doi.org/10.1016/j.stem.2014.04.010.
5. Schaub, J.R., Malato, Y., Gormond, C., and Willenbring, H. (2014). Evidence against a stem cell origin of new hepatocytes in a common mouse model of chronic liver injury. Cell Rep. *8*, 933–939. https://doi.org/10.1016/j.celrep.2014.07.003.
6. Yanger, K., Knigin, D., Zong, Y., Maggs, L., Gu, G., Akiyama, H., Pikarsky, E., and Stanger, B.Z. (2014). Adult hepatocytes are generated by self-duplication rather than stem cell differentiation. Cell Stem Cell *15*, 340–349. https://doi.org/10.1016/j.stem.2014.06.003.
7. Lu, W.Y., Bird, T.G., Boulter, L., Tsuchiya, A., Cole, A.M., Hay, T., Guest, R.V., Wojtacha, D., Man, T.Y., Mackinnon, A., et al. (2015). Hepatic progenitor cells of biliary origin with liver repopulation capacity. Nat. Cell Biol. *17*, 971–983. https://doi.org/10.1038/ncb3203.
8. Raven, A., Lu, W.Y., Man, T.Y., Ferreira-Gonzalez, S., O'Duibhir, E., Dwyer, B.J., Thomson, J.P., Meehan, R.R., Bogorad, R., Koteliansky, V., et al. (2017). Cholangiocytes act as facultative liver stem cells during impaired hepatocyte regeneration. Nature *547*, 350–354. https://doi.org/10.1038/nature23015.
9. Pu, W., Zhu, H., Zhang, M., Pikiolek, M., Ercan, C., Li, J., Huang, X., Han, X., Zhang, Z., Lv, Z., et al. (2023). Bipotent transitional liver progenitor cells contribute to liver regeneration. Nat. Genet. *55*, 651–664. https://doi.org/10.1038/s41588-023-01335-9.
10. Deng, X., Zhang, X., Li, W., Feng, R.X., Li, L., Yi, G.R., Zhang, X.N., Yin, C., Yu, H.Y., Zhang, J.P., et al. (2018). Chronic Liver Injury Induces Conversion of Biliary Epithelial Cells into Hepatocytes. Cell Stem Cell *23*, 114–122.e3. https://doi.org/10.1016/j.stem.2018.05.022.
11. Noël, R. (1922). Recherches histo-physiologiques sur la cellule hépatique des mammifères (Univ. de Paris.).
12. Martini, T., Naef, F., and Tchorz, J.S. (2023). Spatiotemporal Metabolic Liver Zonation and Consequences on Pathophysiology. Annu. Rev.

Pathol. *18*, 439–466. https://doi.org/10.1146/annurev-pathmechdis-031521-024831.

13. Santos, A.A., Delgado, T.C., Marques, V., Ramirez-Moncayo, C., Alonso, C., Vidal-Puig, A., Hall, Z., Martínez-Chantar, M.L., and Rodrigues, C.M.P. (2024). Spatial metabolomics and its application in the liver. Hepatology *79*, 1158–1179. https://doi.org/10.1097/hep.0000000000000341.
14. Colnot, S., and Perret, C. (2011). Liver Zonation. In Molecular Pathology of Liver Diseases, S. Monga, ed. (Springer Science). https://doi.org/10.1007/978-1-4419-7107-4_2.
15. Cunningham, R.P., and Porat-Shliom, N. (2021). Liver Zonation - Revisiting Old Questions With New Technologies. Front. Physiol. *12*, 732929. https://doi.org/10.3389/fphys.2021.732929.
16. Paris, J., and Henderson, N.C. (2022). Liver zonation, revisited. Hepatology *76*, 1219–1230. https://doi.org/10.1002/hep.32408.
17. Halpern, K.B., Shenhav, R., Matcovitch-Natan, O., Toth, B., Lemze, D., Golan, M., Massasa, E.E., Baydatch, S., Landen, S., Moor, A.E., et al. (2017). Single-cell spatial reconstruction reveals global division of labor in the mammalian liver. Nature *542*, 352–356. https://doi.org/10.1038/nature21065.
18. Xu, J., Guo, P., Hao, S., Shangguan, S., Shi, Q., Volpe, G., Huang, K., Zuo, J., An, J., Yuan, Y., et al. (2024). A spatiotemporal atlas of mouse liver homeostasis and regeneration. Nat. Genet. *56*, 953–969. https://doi.org/10.1038/s41588-024-01709-7.
19. Benhamouche, S., Decaens, T., Godard, C., Chambrey, R., Rickman, D.S., Moinard, C., Vasseur-Cognet, M., Kuo, C.J., Kahn, A., Perret, C., and Colnot, S. (2006). Apc tumor suppressor gene is the "zonation-keeper" of mouse liver. Dev. Cell *10*, 759–770. https://doi.org/10.1016/j.devcel.2006.03.015.
20. Colnot, S., and Perret, C. (2010). Liver zonation. In Molecular Pathology of Liver Diseases, S.P.S. Monga, ed. (Springer), pp. 7–16.
21. Wang, B., Zhao, L., Fish, M., Logan, C.Y., and Nusse, R. (2015). Self-renewing diploid Axin2(+) cells fuel homeostatic renewal of the liver. Nature *524*, 180–185. https://doi.org/10.1038/nature14863.
22. May, S., Müller, M., Livingstone, C.R., Skalka, G.L., Walsh, P.J., Nixon, C., Hedley, A., Shaw, R., Clark, W., Vande Voorde, J., et al. (2023). Absent expansion of AXIN2+ hepatocytes and altered physiology in Axin2CreERT2 mice challenges the role of pericentral hepatocytes in homeostatic liver regeneration. J. Hepatol. *78*, 1028–1036. https://doi.org/10.1016/j.jhep.2023.01.009.
23. Sun, T., Pikiolek, M., Orsini, V., Bergling, S., Holwerda, S., Morelli, L., Hoppe, P.S., Planas-Paz, L., Yang, Y., Ruffner, H., et al. (2020). AXIN2^{+} Pericentral Hepatocytes Have Limited Contributions to Liver Homeostasis and Regeneration. Cell Stem Cell *26*, 97–107.e6. https://doi.org/10.1016/j.stem.2019.10.011.
24. Font-Burgada, J., Shalapour, S., Ramaswamy, S., Hsueh, B., Rossell, D., Umemura, A., Taniguchi, K., Nakagawa, H., Valasek, M.A., Ye, L., et al. (2015). Hybrid Periportal Hepatocytes Regenerate the Injured Liver without Giving Rise to Cancer. Cell *162*, 766–779. https://doi.org/10.1016/j.cell.2015.07.026.
25. He, L., Li, Y., Li, Y., Pu, W., Huang, X., Tian, X., Wang, Y., Zhang, H., Liu, Q., Zhang, L., et al. (2017). Enhancing the precision of genetic lineage tracing using dual recombinases. Nat. Med. *23*, 1488–1498. https://doi.org/10.1038/nm.4437.
26. Pu, W., Zhang, H., Huang, X., Tian, X., He, L., Wang, Y., Zhang, L., Liu, Q., Li, Y., Li, Y., et al. (2016). Mfsd2a+ hepatocytes repopulate the liver during injury and regeneration. Nat. Commun. *7*, 13369. https://doi.org/10.1038/ncomms13369.
27. Ang, C.H., Hsu, S.H., Guo, F., Tan, C.T., Yu, V.C., Visvader, J.E., Chow, P.K.H., and Fu, N.Y. (2019). Lgr5^{+} pericentral hepatocytes are self-maintained in normal liver regeneration and susceptible to hepatocarcinogenesis. Proc. Natl. Acad. Sci. USA *116*, 19530–19540. https://doi.org/10.1073/pnas.1908099116.
28. Lin, Y.H., Wei, Y., Zeng, Q., Wang, Y., Pagani, C.A., Li, L., Zhu, M., Wang, Z., Hsieh, M.H., Corbitt, N., et al. (2023). IGFBP2 expressing midlobular hepatocytes preferentially contribute to liver homeostasis and regeneration. Cell Stem Cell *30*, 665–676.e4. https://doi.org/10.1016/j.stem.2023.04.007.
29. Wei, Y., Wang, Y.G., Jia, Y., Li, L., Yoon, J., Zhang, S., Wang, Z., Zhang, Y., Zhu, M., Sharma, T., et al. (2021). Liver homeostasis is maintained by midlobular zone 2 hepatocytes. Science *371*, eabb1625. https://doi.org/10.1126/science.abb1625.
30. He, L., Pu, W., Liu, X., Zhang, Z., Han, M., Li, Y., Huang, X., Han, X., Li, Y., Liu, K., et al. (2021). Proliferation tracing reveals regional hepatocyte generation in liver homeostasis and repair. Science *371*, eabc4346. https://doi.org/10.1126/science.abc4346.
31. He, S., Guo, Z., Zhou, M., Wang, H., Zhang, Z., Shi, M., Li, X., Yang, X., and He, L. (2023). Spatial-temporal proliferation of hepatocytes during pregnancy revealed by genetic lineage tracing. Cell Stem Cell *30*, 1549–1558.e5. https://doi.org/10.1016/j.stem.2023.09.002.
32. Lin, S., Nascimento, E.M., Gajera, C.R., Chen, L., Neuhöfer, P., Garbuzov, A., Wang, S., and Artandi, S.E. (2018). Distributed hepatocytes expressing telomerase repopulate the liver in homeostasis and injury. Nature *556*, 244–248. https://doi.org/10.1038/s41586-018-0004-7.
33. Leushacke, M., Tan, S.H., Wong, A., Swathi, Y., Hajamohideen, A., Tan, L.T., Goh, J., Wong, E., Denil, S.L.I.J., Murakami, K., and Barker, N. (2017). Lgr5-expressing chief cells drive epithelial regeneration and cancer in the oxyntic stomach. Nat. Cell Biol. *19*, 774–786. https://doi.org/10.1038/ncb3541.
34. Chin, C.F., Galam, D.L., Gao, L., Tan, B.C., Wong, B.H., Chua, G.-L., Loke, R.Y., Lim, Y.C., Wenk, M.R., Lim, M.-S., et al. (2023). Blood-derived lysophospholipid sustains hepatic phospholipids and fat storage necessary for hepatoprotection in overnutrition. J. Clin. Invest. *133*, e171267. https://doi.org/10.1172/JCI171267.
35. Fu, N.Y., Rios, A.C., Pal, B., Law, C.W., Jamieson, P., Liu, R., Vaillant, F., Jackling, F., Liu, K.H., Smyth, G.K., et al. (2017). Identification of quiescent and spatially restricted mammary stem cells that are hormone responsive. Nat. Cell Biol. *19*, 164–176. https://doi.org/10.1038/ncb3471.
36. Su, Q., Kim, S.Y., Adewale, F., Zhou, Y., Aldler, C., Ni, M., Wei, Y., Burczynski, M.E., Atwal, G.S., Sleeman, M.W., et al. (2021). Single-cell RNA transcriptome landscape of hepatocytes and non-parenchymal cells in healthy and NAFLD mouse liver. iScience *24*, 103233. https://doi.org/10.1016/j.isci.2021.103233.
37. Bravo Gonzalez-Blas, C., Matetovici, I., Hillen, H., Taskiran, I.I., Vandepoel, R., Christiaens, V., Sansores-Garcia, L., Verboven, E., Hulselmans, G., Poovathingal, S., et al. (2024). Single-cell spatial multi-omics and deep learning dissect enhancer-driven gene regulatory networks in liver zonation. Nat. Cell Biol. *26*, 153–167. https://doi.org/10.1038/s41556-023-01316-4.
38. Mitchell, C., and Willenbring, H. (2008). A reproducible and well-tolerated method for 2/3 partial hepatectomy in mice. Nat. Protoc. *3*, 1167–1170. https://doi.org/10.1038/nprot.2008.80.
39. Hoehme, S., Brulport, M., Bauer, A., Bedawy, E., Schormann, W., Hermes, M., Puppe, V., Gebhardt, R., Zellmer, S., Schwarz, M., et al. (2010). Prediction and validation of cell alignment along microvessels as order principle to restore tissue architecture in liver regeneration. Proc. Natl. Acad. Sci. USA *107*, 10371–10376. https://doi.org/10.1073/pnas.0909374107.
40. Planas-Paz, L., Orsini, V., Boulter, L., Calabrese, D., Pikiolek, M., Nigsch, F., Xie, Y., Roma, G., Donovan, A., Marti, P., et al. (2016). The RSPO-LGR4/5-ZNRF3/RNF43 module controls liver zonation and size. Nat. Cell Biol. *18*, 467–479. https://doi.org/10.1038/ncb3337.
41. Wang, S., Wang, X., Shan, Y., Tan, Z., Su, Y., Cao, Y., Wang, S., Dong, J., Gu, J., and Wang, Y. (2024). Region-specific cellular and molecular basis of liver regeneration after acute pericentral injury. Cell Stem Cell *31*, 341–358.e7. https://doi.org/10.1016/j.stem.2024.01.013.
42. Ruz-Maldonado, I., Gonzalez, J.T., Zhang, H., Sun, J., Bort, A., Kabir, I., Kibbey, R.G., Suárez, Y., Greif, D.M., and Fernández-Hernando, C.

(2024). Heterogeneity of hepatocyte dynamics restores liver architecture after chemical, physical or viral damage. Nat. Commun. *15*, 1247. https://doi.org/10.1038/s41467-024-45439-0.

43. Rios, A.C., Fu, N.Y., Lindeman, G.J., and Visvader, J.E. (2014). In situ identification of bipotent stem cells in the mammary gland. Nature *506*, 322–327. https://doi.org/10.1038/nature12948.
44. Mae, M.A., He, L., Nordling, S., Vazquez-Liebanas, E., Nahar, K., Jung, B., Li, X., Tan, B.C., Chin Foo, J., Cazenave-Gassiot, A., et al. (2021). Single-Cell Analysis of Blood-Brain Barrier Response to Pericyte Loss. Circ. Res. *128*, e46–e62. https://doi.org/10.1161/CIRCRESAHA.120.317473.
45. Li, W.C., Ralphs, K.L., and Tosh, D. (2010). Isolation and culture of adult mouse hepatocytes. Methods Mol. Biol. *633*, 185–196. https://doi.org/10.1007/978-1-59745-019-5_13.
46. Liao, Y., Smyth, G.K., and Shi, W. (2019). The R package Rsubread is easier, faster, cheaper and better for alignment and quantification of RNA sequencing reads. Nucleic Acids Res. *47*, e47. https://doi.org/10.1093/nar/gkz114.
47. Chen, Y., Lun, A.T.L., and Smyth, G.K. (2016). From reads to genes to pathways: differential expression analysis of RNA-Seq experiments using Rsubread and the edgeR quasi-likelihood pipeline. F1000Res. *5*, 1438. https://doi.org/10.12688/f1000research.8987.2.
48. Robinson, M.D., and Oshlack, A. (2010). A scaling normalization method for differential expression analysis of RNA-seq data. Genome Biol. *11*, R25. https://doi.org/10.1186/gb-2010-11-3-r25.
49. Ritchie, M.E., Phipson, B., Wu, D., Hu, Y., Law, C.W., Shi, W., and Smyth, G.K. (2015). limma powers differential expression analyses for RNA-sequencing and microarray studies. Nucleic Acids Res. *43*, e47. https://doi.org/10.1093/nar/gkv007.
50. Hao, Y., Hao, S., Andersen-Nissen, E., Mauck, W.M., 3rd, Zheng, S., Butler, A., Lee, M.J., Wilk, A.J., Darby, C., Zager, M., et al. (2021). Integrated analysis of multimodal single-cell data. Cell *184*, 3573–3587.e29. https://doi.org/10.1016/j.cell.2021.04.048.

STAR★METHODS

KEY RESOURCES TABLE

REAGENT or RESOURCE	SOURCE	IDENTIFIER
Antibodies		
Mouse monoclonal anti-E-cadherin antibody	BD Biosciences	Cat# 610182; RRID: AB_397581
Mouse purified anti-glutamine synthetase antibody	BD Biosciences	Cat# 610517; RRID: AB_397879
Rabbit polyclonal anti-Cyp2e1 antibody	Sigma	Cat# HPA009128; RRID: AB_1078613
Rabbit monoclonal anti-Cyclin D1 antibody	Abcam	Cat# ab16663; RRID: AB_443423
Rabbit polyclonal anti-Hal antibody	Sigma	Cat# HPA038547: RRID: AB_10669541
Mouse monoclonal anti-Gls2 antibody	Abcepta	Cat# AM8595b; RRID: AB_3097731
Rabbit polyclonal anti-RFP antibody	Rockland	Cat# 600-401-379; RRID: AB_2209751
Goat polyclonal anti-RFP antibody	Rockland	Cat# 200-101-379; RRID: AB_2744552
Chicken polyclonal anti-GFP antibody	Abcam	Cat# ab13970; RRID: AB_300798
Mouse purified anti-BrdU antibody (Clone B44)	BD Biosciences	Cat# 347580; RRID: AB_400326
PE/Cy7 anti-mouse CD133 aantibody (Clone 315-2C11)	Biolegend	Cat# 141210; RRID: AB_2564069
Alexa Fluor 647 anti-mouse/human CD324 (E-cadherin) antibody (Clone DECMA-1)	Biolegend	Cat# 147308; RRID AB_2563955
Bacterial and virus strains		
DH5alpha competent cells	Thermo Fisher Scientific	Cat# 18265017
Chemicals, peptides, and recombinant proteins		
Doxycyclin hyclate	Biosynth	Cat# 24390-14-5; Batch number: AA226081801
Tamoxifen	Sigma	Cat# T5648; CAS Number: 10540-29-1
Carbon tetrachloride (CCl4), 99+%, Spectrophotometric grade	ACROS Organics	Cat# AC167725000; Kind gift from Prof. Go Mei Lin
Sunflower seed oil from *Helianthus annuus*	Sigma Aldrich	Cat# S5007-1L CAS Number: 8001-21-6
N-Nitrosodiethylamine (Diethylnitrosamine, DEN)	Sigma	Cat# NO258-1G; Lot number: MKCB0796V
Mouse IgG Blocking Reagent	Vector Laboratories	Cat# MKB-2213; Lot number: ZE1226
Triton™ X-100	Sigma	Cat# T8787; Lot number: MKBW8386V
Horse serum	N/A	N/A
4′,6-Diamidino-2-phenylindole dihydrochloride (DAPI)	Invitrogen	Cat# D9542 CAS Number: 28718-90-3
7-Aminoactinomycin D (7AAD)	Sigma Aldrich	Cat#A9400 CAS Number: 7240-37-1
Deoxyribonuclease I (DNAse I)	Worthington Biochemical Corp	Cat# LS002140 CAS Number: 9003-98-9
5-Bromo-2′-Deoxyuridine (BrdU)	Sigma	Cat# 10280879001 CAS Number: 59-14-3
Liver Perfusion Medium (1x)	Gibco	Cat# 17701-038; Lot number 1960305
Fetal Bovine Serum	Sigma Aldrich	Cat# 12003C
Collagenase, Type 1	Worthington	Cat# LS004196
IgG from rat serum	Sigma	Cat#I4131; Lot number SLBF6029V
GoScript Reverse Transcription Kit	Promega	Cat# A5000
SYBR™ Green PCR Master Mix	Thermo Fisher Scientific	Cat# 4309155
RNeasy™ Micro Kit	Qiagen	Cat# 74004
Critical commercial assays		
Click-iT™ EdU Cell Proliferation Kit for Imaging, Alexa Fluor™ 647 dye	Invitrogen	Cat# C10340

(*Continued on next page*)

Continued

REAGENT or RESOURCE	SOURCE	IDENTIFIER
Deposited data		
Bulk RNA-seq data of hepatocytes isolated from *Cyp2e1/TetO-Cre/R26-Tomato* and *Lgr5-rtTA-IRES-GFP* mice	Reviewer's token: **etknqwqspxajbux**	GEO accession number: GSE268663
Software and algorithms		
ImageJ	Fiji	RRID: SCR_003070 URL: https://imagej.net/
Leica Application Suite X	Leica Microsystems GmbH	RRID: SCR_013673 URL: https://www.leica-microsystems.com/products/microscope-software/details/product/leica-las-x-ls/
GraphPad Prism 10	GraphPad Software	RRID: SCR_002798
FlowJo	Tree Star	RRID: SCR_008520 URL: https://www.flowjo.com/solutions/flowjo
Mus musculus gene information	NCBI	ftp://ftp.ncbi.nlm.nih.gov
R packages Rsubread, limma and edgeR	Bioconductor	RRID: SCR_006442
R package Seurat	CRAN	RRID: SCR_003005
Experimental models: Organisms/strains		
Mouse: FVB/NJ	The Jackson Laboratory	ISMR Cat# JAX:001800, RRID:IMSR_JAX:001800
Mouse: C57BL/6J	The Jackson Laboratory	IMSR Cat# JAX:000664, RRID:IMSR_JAX:000664
Mouse: *Lgr5-rtTA-IRES-GFP*	Ang et al.[27]	N/A
Mouse: *B6.Cg-Gt(ROSA)26Sor$^{tm9(CAG-tdTomato)Hze}$/J*	The Jackson Laboratory	ISMR Cat# JAX:007909, RRID:IMSR_JAX:007909
Mouse: *B6; C-Tg(tetO-cre)LC1Bjd/BjdCnrm*	Heidelberg University, Germany	A gift from Dr. K. Schönig
Mouse: *Cyp2e1-P2A-rtTA*	This paper	N/A
Mouse: *Gls2-P2A-rtTA*	This paper	N/A
Mouse: Ccnd1-EGFP-P2A-rtTA3	This paper	N/A
Mouse: *B6.129P2-Gt(ROSA)26Sor$^{tm1(DTA)Lky}$/J*	The Jackson Laboratory	ISMR Cat# JAX:009669, RRID:IMSR_JAX:009669
Mouse: *Mfsd2a-CreERT2*	Duke-NUS Medical School	A gift from Prof. David Silver
Mouse: *Lgr5-2A-CreERT2*	A*STAR Institute of Medical Biology, Singapore	A gift from Dr. Nick Barker
Oligonucleotides		
Genotyping primers of the Lgr5-rtTA-IRES-GFP line: (1). 5′-tctgctcccagtctcgggcaccatgg-3' (2). 5′-tggtaggtgtctctctrtcctctt-3′	Integrated DNA Technologies	N/A
Genotyping primers of the Cyp2e1-P2A-rtTA line: (1). 5′-tcatcagcactgttgtctcttcta-3' (2). 5′-gctgcctgctgacgctcttgacgat-3′ (3). 5′-gataggaactccatatgcttggca-3′	Integrated DNA Technologies	N/A
Genotyping primers of the Gls2-P2A-rtTA line: (1). 5′-gagtcctctttgcctaactgtga-3' (2). 5′-ctgtagctagctctgctcaggtat-3′ (3). 5′-ttcttcaacatctcctgcttgctt-3′	Integrated DNA Technologies	N/A
Genotyping primers of the Ccnd1-EGFP-P2A-rtTA3 line: (1). 5′-ctctttgcgggtgccactacttgg-3' (2). 5′-gcggacttgaagaagtcgtg-3′ (3). 5′-gcctctggctaaacaaggacc-3′	Integrated DNA Technologies	N/A
Genotyping primers of the TetO-cre mouse line: (1). 5′-gcggtctggcagtaaaaactatc-3' (2). 5′-gtgaaacagcattgctgtcactt-3′	Integrated DNA Technologies	N/A
Genotyping primers of the Rosa26-tdTomato mouse line: (1). 5′-aagggagctgcagtggagta-3' (2). 5′-ccgaaaatctgtgggaagtc-3′ (3). 5′-ggcattaaagcagcgtatcc-3′ (4). 5′-ctgttcctgtacggcatgg-3′	Integrated DNA Technologies	N/A

(*Continued on next page*)

Continued

REAGENT or RESOURCE	SOURCE	IDENTIFIER
Genotyping primers of the Lgr5-T2A-CreER line: (1). 5′-agcctatgacttgccttcca-3’ (2). 5′-cggttattcaacttgcacca-3′ (3). 5′-tgacttgatggctttccttc-3′	Integrated DNA Technologies	N/A
Genotyping primers of the Msfd2a-CreER line: (1). 5′-ttggctggaggcgcaggcccgaacc-3’ (2). 5′-tcgttgcatcgaccggtaatgcaggc-3′	Integrated DNA Technologies	N/A
Genotyping primers of the DTA line: (1). 5′-ccaaagtcgctctgagttgttatc-3’ (2). 5′-gagcgggagaaatggatatg-3′ (3). 5′-cgacctgcaggtcctcg-3′ (4). 5′-ctcgagtttgtccaattatgtcac-3′	Integrated DNA Technologies	N/A

EXPERIMENTAL MODEL AND STUDY PARTICIPANT DETAILS

For the generation of *Gls2-P2A-rtTA*, *Cyp2e1-P2A-rtTA* and *Ccnd1-EGFP-P2A-rtTA3* knockin mice, the TGA stop codon of the *Gls2* or *Cyp2e1* gene was replaced with a *P2A-rtTA3* or *EGFP-P2A-rtTA3* cassette by CRISPR/Cas9-mediated genome engineering. At least three different founders were generated for each line. Offsprings from each founder were crossed to *TetO-Cre*/*R26-Tomato* reporter mice[35,43] for testing. Immunofluorescence staining of liver sections using liver zonation markers showed that all founders exhibited similar Tomato expression patterns. Only one founder was chosen for lineage tracing studies for each line. We also utilized three other previously reported mouse lines— *Lgr5-rtTA-IRES-GFP,*[31] *Lgr5-T2A-CreER*[33] and *Msfd2a-CreER*[44] mice—and crossed them to the aforementioned *TetO-Cre*/*R26-Tomato* reporter mice for experiments. All mice were maintained in specific pathogen free (SPF) facility and handled in accordance with protocols approved by the Institute animal care and use committee at SingHealth or WEHI. Only male mice were used for RNA-sequencing experiments. A mix of male and female mice were used for all other experiments with no gender-bias differences observed.

METHOD DETAILS

Doxycycline and tamoxifen administration

For labeling and tracing of *Cyp2e1*$^{+}$, *Gls2*$^{+}$, *Lgr5*$^{+}$, and *Ccnd1*$^{+}$ hepatocytes in *Cyp2e1*$^{KI/+}$*;TetO-Cre*$^{T/+}$*;R26-Tomato*$^{KI/+}$, *Gls2*$^{KI/+}$*; TetO-Cre*$^{T/+}$*;R26-Tomato*$^{KI/+}$, *Lgr5*$^{T/+}$*;TetO-Cre*$^{T/+}$*;R26-Tomato*$^{KI/+}$ and *Ccnd1*$^{KI/+}$*;TetO-Cre*$^{T/+}$*;R26-Tomato*$^{KI/+}$ lines respectively, adult mice at 7–9 weeks old were fed with Doxycycline (DOX) feed and drinking water containing 1 mg/ml DOX and 10 mg/mL sucrose for 7 continuous days. For quick labeling of Cyp2e1-, Gls2-, and Lgr5-descendant hepatocytes in respective lines in young pups, pups at P7 or P21 were pulsed with one dose of DOX at 50 μg/g body weight via intraperitoneal (IP) injection. For low-labeling of Gls2 hepatocytes in *Gls2*$^{KI/+}$*;TetO-Cre*$^{T/+}$*;R26-Tomato*$^{KI/+}$ line, 7-8 week-old adult mice were pulsed with one dose of 0.5 mg DOX via IP injection.

For deletion of *Cyp2e1* cells, adult *Cyp2e1*$^{KI/+}$*;R26-DTA*$^{KI/+}$*;TetO-Cre*$^{T/+}$*;R26-Tomato*$^{KI/+}$ mice were fed with DOX feed and drinking water containing 1 mg/ml DOX and 10 mg/ml sucrose for 3 days. For labeling and tracing of *Lgr5*$^{+}$ and *Msfd2a*$^{+}$ hepatocytes in *Lgr5CreERT2*$^{KI/KI}$*;R26-Tomato*$^{KI/KI}$ and *Msfd2a-CreERT2*$^{KI/+}$*;R26-Tomato*$^{KI/+}$ lines, 7-9 weeks-old adult mice were given 2 doses of Tamoxifen (TAM) at 100 μg per gram of body weight via IP injection for 2 alternate days. All mice were rested for 7 days after DOX or TAM treatments prior to conducting any subsequent procedures.

Liver injury models

Two-third partial hepatectomy (PH) was performed as previously described.[27] During the surgery, the resected median and left lateral lobes were collected for analysis. Regenerated right and caudate lobes were collected at 14 days after the surgery for analysis. PH procedure was performed in the morning for all mice. For acute DEN-induced liver injuries, adult male mice were IP injected with 3 doses of DEN, diluted in PBS at 100 μg/g body weight, 1 dose per week for 3 weeks. For CCl_4-induced liver injuries, adult mice were IP injected with 10 doses of CCl_4 at 1 μL/g body weight, diluted in sunflower seed oil at 1:3 dilution, over a period of 3 weeks. For chronic DDC-induced periportal injuries, both male and female adult mice were fed with rodent diet containing 0.1% DDC for a desired period of time after DOX or TAM pulsing; upon completion of each chemical treatment, mice were given normal food and drinking water for a desired period of time to allow recovery, according to experimental designs.

Histology and immunofluorescence staining

Livers were harvested and immediately fixed in 4% paraformaldehyde (PFA) 24 h at room temperature, followed by 24 h at 4°C. Tissues were embedded in paraffin and sectioned at a thickness of 4μm for immunofluorescence staining. Slides were dewaxed at 60°C for at least an hour and dehydrated through a descending series of ethanol to water. Heat-induced epitope retrieval was carried out for 10 min in a pressure cooker at the highest pressure with slides submerged in either sodium citrate (pH6) solution or Tris-EDTA (pH9) solution. Slides were cooled down on ice and washed with tap water several times. Following two washes with PBS containing 0.1% Triton X-100, the slides were blocked in PBS containing 10% horse serum, 0.1% Triton X-100 and 2% mouse on mouse (M. O. M) blocking reagent for 30 min. They were then washed with PBS containing 0.01% Triton X-100 thrice and incubated with primary antibodies diluted in PBS containing 0.01% Triton X-100 and 1% horse serum at 4°C overnight. After three washes with PBS containing 0.01% Triton X-100, slides were incubated with secondary antibodies in PBS containing 0.01% Triton X-100 and 1% horse serum at room temperature for an hour. They were then washed with PBS containing 0.01% Triton X-100 thrice and stained with DAPI in PBS for 5 min, before mounting on an anti-fade mounting medium and storing at 4°C in the dark. Images were acquired with a Leica TCS SP8 confocal microscope.

BrdU and EdU administration

BrdU was administered to the mice via drinking water at 1 mg/mL. EdU (Click-iT EdU Imaging Kits, Invitrogen) was administered to the mice via drinking water at 0.3 mg/mL. Both BrdU and EdU water were refreshed daily during the treatment.

Western blot analysis

The primary antibodies used for western blot are listed in key resources table. A small piece of liver tissue was homogenized in lysis buffer 50 mM NaCl, 50 mM Tris-HCl, pH 7.3, 0.25 mM EDTA, pH 8.0, 1% sodium deoxycholate, 1% Triton X-100, 0.2% sodium fluoride and 0.1% sodium orthovanadate) with protease and phosphatase inhibitor cocktail (Roche, Manheim, Germany). The lysates were then resolved on 10% SDS-PAGE and transferred onto a PVDF membrane. Following blocking of the PVDF membrane with 5% non-fat milk in wash buffer (TBS, 0.01% Triton X-100) for 1 h at 37°C, immunoblotting was carried out by incubation with specific primary antibodies at 4°C overnight. Following this, the membrane was washed thrice with wash buffer, and incubated with HRP-conjugate secondary antibodies for 1 h at room temperature. Western blot images were captured using ChemiDoc Imager (Bio-Rad Laboratories, US).

FACS sorting of hepatocytes and RNA-seq

Adult male *Cyp2e1*$^{KI/+}$*;TetO-Cre*$^{T/+}$*;R26-Tomato*$^{KI/+}$ mice were treated with DOX food and drinking water for 7 continuous days prior to FACS sorting. Tomato^{+} and Tomato^{-} hepatocytes from *Cyp2e1*$^{KI/+}$*;TetO-Cre*$^{T/+}$*;R26-Tomato*$^{KI/+}$ mice and GFP^{+} hepatocytes from *Lgr5-rtTA-IRES-GFP*$^{T/+}$ mice were isolated from the liver of adult male mice by a modified two-step collagenase perfusion technique[45] for FACS sorting. For this, mice were anesthetized by 2% isoflurane inhalation. An incision was made through their abdominal skin and muscle layer to expose the liver. The inferior vena cava was cut, and the liver was perfused via portal vein with Liver Perfusion Medium (Gibco #17701038), followed by collagenase solution containing type III collagenase (Worthington). After sufficient digestion, the liver was removed and hepatocytes were dispersed into suspension in DMEM medium with 5% FBS and filtered through 70μm cell strainer. Hepatocytes were washed twice by centrifugation at 50*g* for 5 min and resuspended in DMEM medium with 5% FBS. Viable hepatocytes were then enriched by Percoll gradient centrifugation. Hepatocytes in suspension were stained with anti-CD133 antibodies to exclude contamination of cholangiocytes and with DAPI to exclude dead cells.

Total RNA extraction was performed on FACS-purified Cype21-RFP^{+} and RFP^{-}, and Lgr5-GFP^{+} and GFP^{-} hepatocytes according to manufacturer's protocol (Qiagen). Total RNA was converted to cDNA using GoScript Reverse Transcription Kit (Promega). SYBR green qPCR master mix (Bio-Rad) was used for quantitative RT-PCR. The sequences of PCR primers used in this study are listed in key resources table. RNA libraries for bulk RNA sequencing were generated based on TruSeq RNA sample preparation v2 guide and then sequenced on Illumina NovaSeq6000 platform.

RNA-seq data analysis

About 20–35 million 150 bp paired end reads were obtained for each bulk RNA sample. Reads were mapped to the mouse genome (mm39) using the align function and were counted using the featureCounts function in Rsubread (v2.10.2) package.[46] Differential expression analysis was performed for Cyp2e1^{+} vs. Cyp2e1^{-} hepatocyte samples and Lgr5^{+} vs. Lgr5^{-} hepatocyte samples, respectively. Lowly expressed genes were filtered out using the filterByExpr function in edgeR (v3.38.1) package,[47] and normalization was done using the TMM[48] normalization method in edgeR. Subsequently, differential expression analysis was performed using the edgeR quasi-likelihood pipeline.[47] The glmTreat method in edgeR with a log2 fold change threshold of 1 was further used to reduce the number of differentially-expressed (DE) genes. The kegga function in limma (v3.55.5) package[49] was performed on the DE genes for KEGG pathway enrichment analysis.

scRNA-seq data analysis

Two public scRNA-seq datasets—accession numbers GSE166504 [36] and GSE218472 [37]— were downloaded from Gene Expression Omnibus. We first obtained data for hepatocytes from the two public datasets. For scRNA-seq data of Su et al.,[36] six hepatocyte

samples (Hepatocyte_Chow) were extracted based on cell type annotation provided by the authors. For scRNA-seq data of Bravo Gonzalez-Blas et al.,[37] hepatocytes data were obtained by integrating snRNA-seq data of four mouse liver samples and scMultiome (RNA) data of two mouse liver samples using Seurat (v4.1.1)[50] integration pipeline without removing any cells. Then, we integrated the hepatocytes of each dataset using the DE genes identified in our bulk RNA-seq data ($Cyp2e1^+$ vs. $Cyp2e1^-$) as anchor genes for the Seurat integration pipeline. For the hepatocyte integration analysis, normalization was performed using the NormalizeData function for each sample. DE genes between $Cyp2e1^+$ and $Cyp2e1^-$ bulk RNA samples were used as anchor genes to obtain the anchors using FindIntegrationAnchors function. The anchors were integrated together by IntegrateData function. The integrated data was then scaled by ScaleData function for dimension reduction analysis. Principal component analysis (PCA) and uniform manifold approximation and projection (UMAP) were performed to obtain the reduced dimensions. Clusters were identified by FindNeighbors and FindClusters. Positive marker genes of different clusters were obtained by using FindAllMarkers function with a log2 fold change threshold of 0.25. Average expression of the up-regulated genes in $Lgr5^+$ bulk RNA samples, compared to $Lgr5^-$ bulk RNA samples, were identified as Lgr5 cell signature for use in scRNA-seq studies.

QUANTIFICATION AND STATISTICAL ANALYSIS

Data, in the Figure legends, Figures and Results, are shown as mean ± standard error of the mean (s.e.m). Value of n stated in the Figure legends represents number of animals analyzed in each experimental group. The Student's t-test using GraphPad Prism (GraphPad Software) was used where applicable, with $p < 0.05$ considered significant.